# DEPARTAMENT OF MATERIALS SCIENCE

TIAGO XAVIER VERÍSSIMO DA SILVA Bachelor of Science in Materials Engineering

Sustainable Energy Harvesting Paper for Interactive Smart Packaging

MASTER IN MATERIALS ENGINEERING NOVA University Lisbon September 2022





# DEPARTAMENT OF MATERIALS SCIENCE

# Sustainable Energy Harvesting Paper for Interactive Smart Packaging

#### **TIAGO XAVIER VERÍSSIMO DA SILVA**

Bachelor of Science in Materials Engineering

Adviser: Doctor Andreia dos Santos,

Senior Researcher of Sensors in ALMASCIENCE

Co-advisers: Doctor Ana Rovisco,

CENIMAT Researcher, Department of Materials Science of NOVA School of Science and Technology

#### **Examination Committee:**

Chair: Doctor Alexandre Velhinho,

Assistant Professor, DCM, FCT-NOVA

Rapporteur: Doctor Rui Igreja,

Assistant Professor, DCM, FCT-NOVA

Adviser: Doctor Andreia dos Santos,

Senior Researcher of Sensors in ALMASCIENCE

Sustainable Energy Hermating Department Interactive Smoot Deckaging
Sustainable Energy Harvesting Paper for Interactive Smart Packaging  Copyright © Tiago Xavier Veríssimo da Silva, NOVA School of Science and Technology, NOVA
University Lisbon.
The NOVA School of Science and Technology and the NOVA University Lisbon have the right,
perpetual and without geographical boundaries, to file and publish this dissertation through
printed copies reproduced on paper or on digital form, or by any other means known or that
may be invented, and to disseminate through scientific repositories and admit its copying and distribution for non-commercial, educational or research purposes, as long as credit is given

to the author and editor.

Dedicado aos meus pais, que me deram liberdade para crescer.

# **A**CKNOWLEDGMENTS

Quero agradecer à professora Elvira Fortunato, ao professor Rodrigo Martins e ao professor João Paulo Borges pelo conjunto de condições favoráveis à realização da minha dissertação.

This work was financed by national funds from FCT - Fundação para a Ciência e a Tecnologia, I.P., in the scope of the projects LA/P/0037/2020, UIDP/50025/2020 and UIDB/50025/2020 of the Associate Laboratory Institute of Nanostructures, Nanomodelling and Nanofabrication – i3N and by the European Union's Horizon 2020 research and Innovation programme under grant agreement N° 101008701 (EMERGE).

Quero agradecer também à ALMASCIENCE, ao Cenimat e Cemop pela oportunidade da realização da minha tese nas melhores condições. E à FCT que realmente considero a faculdade rainha e à qual eu associo inúmeras memórias ao longo destes 5 anos.

Quero agradecer muito às minhas orientadoras, Andreia dos Santos e Ana Rovisco, por tudo o que fizeram para me ajudar, pela simpatia sempre demonstrada comigo, por toda atenção dedicada no trabalho e nas minhas dúvidas. Por acaso este grande passo na minha vida (a finalização do mestrado), coincidiu com outros grandes passos na vida de cada uma, espero que vocês e os seus sejam felizes e que corra sempre tudo bem!

Quero agradecer a todos os que me ajudaram no laboratório, para aperfeiçoar o meu trabalho, especialmente à Maria Morais e à Cristina Gaspar que me ajudaram sempre que eu precisava de resolver algo ou tinha algumas dúvidas um pouco questionáveis.

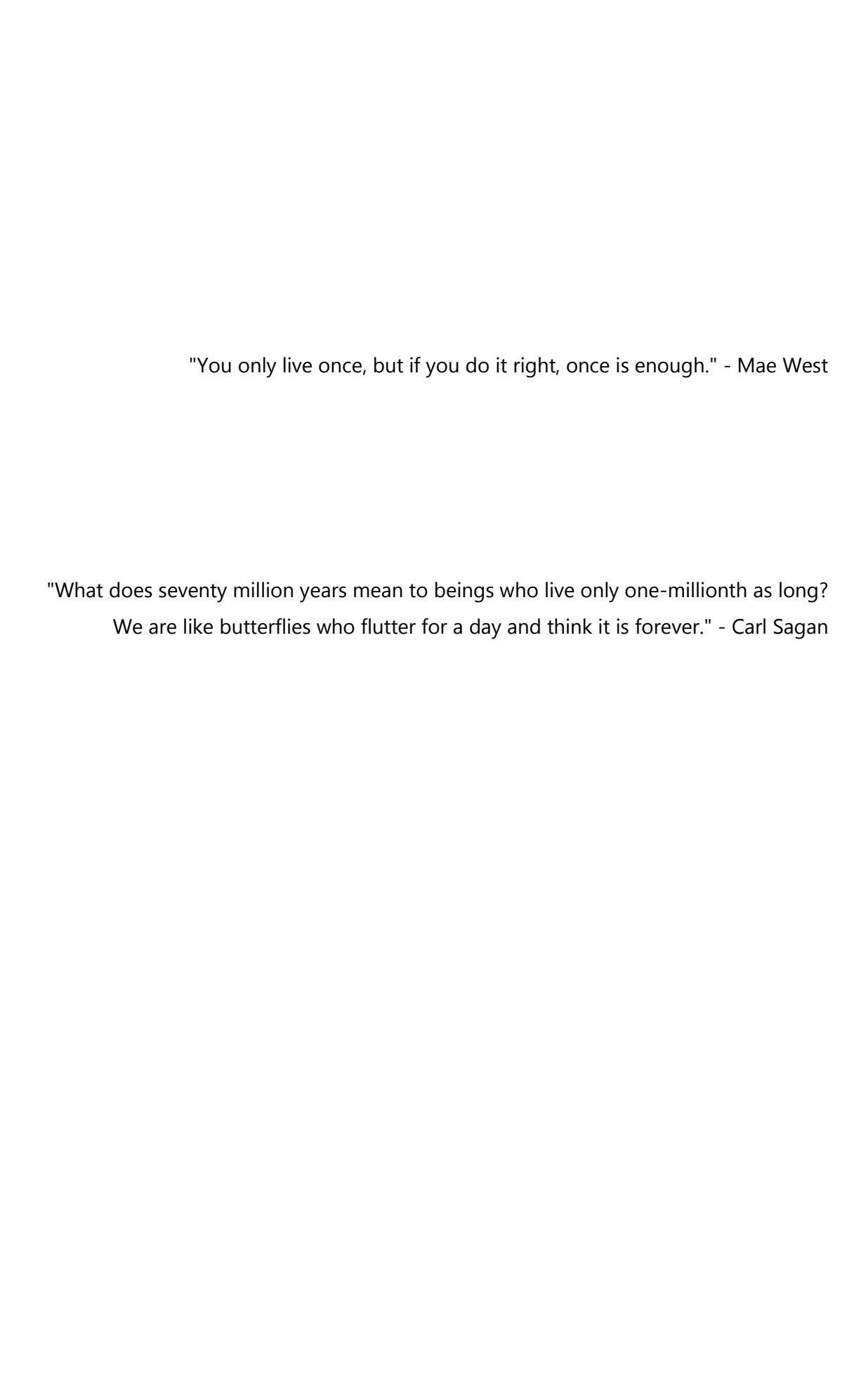
Quero agradecer aos meus grandes amigos da faculdade: Ricardo, Martins, Jorge, Alex, Vítor, António, Carolina, Rita, Manuel, Fialho, Gonçalo, Camecelha. Às incontáveis histórias que tenho com cada um ao longo destes 5 anos, desde as longas sessões de estudo, a todas as saídas, convívios e festas em que tivemos presentes, a vida é uma balança e é preciso equilibrála. Aproveitem tudo miúdos, que a vida vos irá sorrir sempre. ;)

Quero agradecer aos meus ex-colegas de casa André e Margarida, por facilitarem o diaa-dia nos primeiros meses, por todos os momentos de diversão, todos os jantares juntos e especialmente à minha grande amiga Margarida por todas as conversas noite adentro, muito obrigado.

Quero agradecer aos meus grandes amigos de longa data que tenho do Entroncamento: Mota, Manuel, Rafa, Moreira, Lucas, André, Luís, Farinha e Íris, um grande obrigado por tudo o que passamos, sempre que estamos juntos há mais uma memória para a coleção. Que continue assim até ao fim das nossas vidas.

Quero agradecer à minha família, à minha avó, aos meus tios, e especialmente aos meus pais por tudo o que fizeram por mim, todas as condições que me forneceram ao longo dos anos, por tudo o que me ensinaram desde pequeno até ao dia de hoje, todas as oportunidades de viajar e conhecer o mundo, que eu valorizo imenso. Não podia estar mais grato, muito obrigado por tudo! E que passem os anos seguintes onde vocês mais desejem, seja onde for, que importa é sermos felizes!

Todos concluíram para o meu desenvolvimento e para ser a pessoa que eu sou hoje.



## **ABSTRACT**

Interactive Packaging, a subsection of Smart Packaging, relates to packages that interact with the consumer through functional and amusing elements that can be printed labels, wireless communication chips, quick response codes, light or sound systems. These elements frequently require an energy source, with energy harvester devices (EHDs) being a favorable choice.

In the past few years there has been a tendency towards the selection of sustainable, low-cost, widespread, and environmentally friendly materials for smart, self-sustainable, and multifunctional EHDs, while keeping the desired energy harvesting potential. Furthermore, the production method of said EHDs is desirable to be easily scalable and low-cost, allowing mass production.

This work aimed at producing a multifunctional EHD based on paper, to be integrated into interactive packaging. To replace materials commonly used in piezoelectric and triboelectric EHDs, namely the polyethylene terephthalate (PET) substrate with indium tin oxide (ITO) and the polydimethylsiloxane (PDMS) matrix, Navigator and Whatman papers were studied, as well as ethyl cellulose (EC) and carboxymethyl cellulose (CMC). These papers and cellulose matrixes represent more sustainable alternatives that can still offer suitable properties for the development of robust harvesters.

Based on previous works, zinc oxide (ZnO) rods were considered for the EHDs assembly, due to the piezoelectric property allied with the sustainability and wide availability of raw materials.

The ZnO rods were obtained by hydrothermal synthesis assisted by microwave irradiation. Pure ZnO structures were obtained through an easily reproducible, low-cost, and well-controlled synthesis. Various combinations between the two substrates, the three matrices, and the ZnO rods were exploited to maximize the performance of the EHDs.

The best output voltage obtained during this work was from the EHD with ZnO rods mixed in EC deposited in the substrate Whatman between PET/ITO electrodes, which reached an average peak-to-peak voltage of 3.5 V, with a 9 N pushing force.

**Keywords:** smart packaging, energy harvesting, piezoelectric, triboelectric, ZnO, paper, cellulose.

# **RESUMO**

Embalagens Interativas, uma subseção das Embalagens Inteligentes, referem-se a embalagens que interagem com o consumidor através de elementos funcionais e engraçados que podem ser rótulos impressos, chips de comunicação sem fios, códigos de resposta rápida, sistemas de luz ou som. Estes elementos frequentemente requerem uma fonte de energia, sendo os dispositivos coletores de energia (DCEs) uma escolha favorável.

Nos últimos anos tem havido uma tendência, em relação à seleção de materiais sustentáveis, de baixo custo, globalmente difundidos e ecológicos para a produção de DCEs inteligentes, autossustentáveis e multifuncionais, mantendo o potencial de captação de energia desejado. Além disso, é desejável que o método de produção dos referidos DCEs seja facilmente escalável e de baixo custo, permitindo a produção em massa.

Este trabalho teve como objetivo a produção de um DCE multifuncional baseado em papel, para ser integrado em embalagens interativas. Para substituir materiais já usados em DCEs piezoelétricos e triboelétricos como o substrato de politereftalato de etileno (PET) com óxido de índio estanho (ITO) e a matriz de polidimetilsiloxano (PDMS), os papéis Navigator e Whatman foram estudados, bem como etilcelulose (EC) e carboximetilcelulose (CMC), como alternativas mais sustentáveis mantendo ainda as propriedades adequadas para a produção de DCEs robustos.

Com base em trabalhos anteriores, os bastonetes de óxido de zinco (ZnO) foram considerados para a integração em DCEs, devido à propriedade piezoelétrica aliada à sustentabilidade e ampla disponibilidade das matérias-primas.

Os bastonetes de ZnO foram obtidos por síntese hidrotérmica assistida por irradiação de micro-ondas. As estruturas de ZnO puro foram obtidas através de uma síntese facilmente reprodutível, de baixo custo e bem controlada. Várias combinações entre os dois substratos, as três matrizes e os bastonetes de ZnO foram exploradas para maximizar o desempenho dos DCEs.

A melhor tensão de saída obtida durante este trabalho foi do DCE com bastonetes de ZnO misturados em EC depositados no papel Whatman entre elétrodos de PET/ITO, que atingiu uma tensão média pico-a-pico de 3.5 V, com uma força de 9 N.

**Palavras-chave:** embalagens inteligentes/interativas, colheita de energia, piezoelétrico, triboelétrico, ZnO, papel, celulose.



# **CONTENTS**

ACKNO	WLEDG	MENTS	IX
ABSTRA	\CT		XIII
RESUM	o		XV
CONTE	NTS		XVII
LIST OF	FIGURE	<u> </u>	XIX
LIST OF	TABLES	5	XXIII
ACRON	YMS		xxv
MOTIVA	ATION A	AND CONTEXT	XXVII
1 IN	NTRODU	JCTION	1
1.1	Sma	art Packaging	1
1.2	Ene	rgy Harvesters Devices	2
1.3	Piez	zoelectricity	3
1.4	Trib	ooelectricity	3
1.5	Cell	ulose	4
1.6	Piez	zoelectric Materials	5
1.7	Trib	ooelectric Materials	5
2 M	1ATERIA	ALS AND METHODS	7
2.1	Mat	terials	7
2.	1.1	Zinc Oxide Rods Synthesis	7
2.	1.2	PDMS	7
2.	1.3	CMC and EC	8
2.	1.4	ZnO coatings	8
2.	1.5	Substrates	8
2.2	Me	thods	8
2.7	2 1	Screen Printing	8

	2.2.2	Automatic Film Applicator or Coater	9
	2.2.3	Electrical Characterization	9
	2.2.4	Morphological and Structural Characterization	9
3	RESULTS	S AND DISCUSSION	11
	3.1 Ch	aracterization of the zinc oxide rods	11
	3.1.1	Scanning electron microscopy (SEM) of the ZnO rods	11
	3.1.2	Rods Dimensions	12
	3.1.3	X-ray diffraction (XRD) studies of ZnO rods	13
	3.2 Ene	ergy Harvester EHDs	13
	3.2.1	Topographical Characterization of Embedded Substrates	13
	3.2.2	Dimensional Characterization of Embedded Substrates	15
	3.2.3	Opacity and Flexibility of the EHDs	19
	3.3 Ele	ctrical Characterization of the EHDs	20
	3.3.1	Type of EHDs produced	23
	3.3.2	Results	25
4	CONCLU	JSIONS AND FUTURE PERSPECTIVES	31
Bie	BLIOGRAPH	Y	35
	<b>A</b>		4

# LIST OF FIGURES

Figure 1.1 - Working mechanism of the piezoelectric devices under external forces, compression, and decompression, in (a) a device without surface structures and in (b) a device
with pyramidal shapes on its surface. Image of supplementary reference material [31]3
Figure 1.2 - The four different modes of operation of the TENG. In <b>a)</b> the vertical contact-separation mode; <b>b)</b> lateral-sliding mode; <b>c)</b> single-electrode mode; and in <b>d)</b> freestanding triboelectric-layer mode. Image adapted from [27]
Figure 3.1 - SEM images of the ZnO rods synthesised, with different magnifications: a) ×2500 and b) ×500011
Figure 3.2 - Histograms, with a frequency of $n = 150$ , showing <b>a)</b> the length distribution and <b>b)</b> the diameter distribution of the ZnO rods produced in different syntheses (second, eighth and ninth syntheses), for effects of repeatability of the synthesis
Figure 3.3 - XRD diffractogram of ZnO rods. The identification of ZnO was made following ICDD card #36-1451
Figure 3.4 - SEM images from a top viewpoint of several embedded substrates produced. Vertically, the substrates are Whatman (on the left) and Navigator (on the right). Horizontally there is a control (only paper) followed by 3 matrices, CMC, EC and PDMS. Substrates: a) Whatman, b) Navigator, c) Whatman with CMC, d) Navigator with CMC, e) Whatman with EC, f) Navigator with EC, g) Whatman with PDMS, and h) Navigator with PDMS
Figure 3.5 - SEM images from a cross section point of view of several embedded substrates produced. Vertically, the substrates are Whatman (on the left) and Navigator (on the right). Horizontally there is a control followed by 3 matrices, CMC, EC and PDMS. Substrates: a) Whatman, b) Navigator, c) Whatman with CMC, d) Navigator with CMC, e) Whatman with EC, f) Navigator with EC, g) Whatman with PDMS, and h) Navigator with PDMS
Figure 3.6 - Column chart showing the thickness of various embedded substrates produced. The substrates are separated by colours, in blue Whatman and in red Navigator. The paired columns have the control sample followed by 3 matrices, CMC, EC and PDMS (from left to right)
Figure 3.7 - Six photographs, to contrast the transparency in <b>a</b> ) and opaqueness, in <b>c</b> ) and <b>e</b> ), of the EHD produced, and showing the flexibility associated with each one, in <b>b</b> ), <b>d</b> ) and <b>f</b> ).

Comparing the EHD constructed in the previous work [8], with the ones in the present investigation. EHDs displayed: <b>a)</b> and <b>b)</b> , PDMS between the PET/ITO electrodes, <b>c)</b> and <b>d)</b> ,
substrate Whatman, embedded with EC mixed with ZnO rods, between PET/ITO electrodes and lastly, <b>e)</b> and <b>f)</b> , substrate Whatman, embedded with PDMS mixed with ZnO rods, with Ag electrodes
Figure 3.8 - A schematic representation of a regular EHDs' working mechanism. In <b>a)</b> before impact (normal state), in <b>b)</b> while being compressed, in <b>c)</b> totally compressed and in <b>d)</b> while being released. Based on [11]20
Figure 3.9 - Schematic structures of the two types of substrates of the EHD produced. In <b>a)</b> the EHDs build with PET/ITO and in <b>b)</b> the EHDs build with Ag electrodes printed on each side of the substrate. Image not to scale
Figure 3.10 - Example of the output voltage coming from one single impact on the EHD. In <b>a)</b> A representative output peak-to-peak voltage from the EHDs. With close-ups photographs of the impact area, in <b>b)</b> in the normal state and in <b>c)</b> the compressing and releasing22
Figure 3.11 - Six photographs of the EHDs after the deposition and drying phase, prior to assembly. On the left side there is the matrix CMC mixed with ZnO and on the right the matrix EC mixed with ZnO, and in a) and b) both were applied in the substrate Whatman, in c) and d), applied in the substrate Navigator and e) and f) the substrate PET/ITO24
Figure 3.12 - Output peak-to-peak voltage of the EHDs produced with the substrate PET/ITO, starting from the control ones, the two papers and the three matrices solely, and presenting all combinations among them, from left to right25
Figure 3.13 - Output peak-to-peak voltage of the EHDs produced with the substrate PET/ITO and with ZnO rods mixed in the matrices, starting from just the matrices and presenting all combinations between the substrates and these matrices with or without ZnO rods, from left to right
Figure 3.14 - One of the greatest peak-to-peak voltage obtain during this dissertation, being from the substrate Whatman embedded with the matrix EC mixed with ZnO rods, which reached the best output voltage
Figure 3.15 - Output peak-to-peak voltage of the EHDs produced with Ag electrodes. In green the EHDs with solely the substrates. Navigator and Whatman, are presented, in red the EHDs

with the substrates embedded with a matrix are presented and lastly in blue the papers of the papers	-
embedded with the matrix with ZnO rods are presented	.28
Figure 3.16 - A cross section SEM image of the EHD with the matrix CMC embedded in t	the
substrate Whatman with Ag electrodes applied by screen printing	.29
	1
Figure A.1 - Illustrative screen printing scheme of a homemade system [66][66]	
Figure A.2 - Three photographs of the home-made bending machine	2
Figure A.3 - Three photographs of the support for the EHD to be place. In ${f a}$ ) without an EH	HD,
with the force sensor in sight, in <b>b)</b> with an EHD with PET/ITO electrodes, and in <b>c)</b> with an E	HD
with Ag electrodes, both structures made in this dissertation	3
Figure A.4 - Schematic representation of the impact head hitting the EHD. Image not to sca	ale.
	3
Figure A.5 - SEM equipment used for morphological and structural analysis of the EHDs a	and
ZnO rods. In <b>a)</b> the outside of the equipment and in <b>b)</b> the inner drawer to insert the samp	oles
to be analysed	4
Figure A.6 - Six cross section SEM images from the devices with ZnO rods embedded in t	the
matrices. Horizontally the two substrates, Navigator and Whatman, and vertically the th	ree
matrices, PDMS, CMC and EC	7
Figure A.7 - Four photographs of the EHDs build with PDMS mixed with ZnO rods, from t	the
side where the mixture was applied and from the opposite side	8
Figure A.8 - Four photographs of the EHDs build with PDMS deposited on the substrates, ir	ո <b>a)</b>
and <b>c)</b> the substrate Navigator and in <b>b)</b> and <b>d)</b> the substrates Whatman	9
Figure A.9 - Working principle of the hybrid NG, with the wavy substrates, being an exam	ple
of how a EHDs can be built in future works. Image from [32]	9

# LIST OF TABLES

Table A.1 - Global list of the EH	D produced over the course of this thesis	42

# **A**CRONYMS

BaTiO<sub>3</sub> Barium Titanate

CMC Carboxymethyl Cellulose

**DAA** Diacetone Alcohol

**DC** Direct Current

**EC** Ethyl Cellulose

**EHD** Energy Harvester Device

ITO Indium Tin Oxide

PDMS Polydimethylsiloxane

**PENG** Piezoelectric Nanogenerator

**PET** Polyethylene Terephthalate

**PZT** Lead Zirconate Titanate

**SEM** Scanning Electron Microscopy

SLS Sodium Lauryl Sulfate

**TENG** Triboelectric Nanogenerator

wt Weight

XRD X Ray Diffraction

**ZnO** Zinc Oxide

# MOTIVATION AND CONTEXT

The main purpose of this dissertation was the production of an energy harvester device (EHD) based on a composite of zinc oxide (ZnO) structures embedded in paper. The output voltage of the EHD was optimized varying the composition of the composite and the desgin of the EHD. A simple circuit involving a EHD connected to a capacitor and a printed electrochromic element, represents a potential application in smart and interactive packaging. The smart and interactive packaging field has experienced significant advances in recent years, enabling in this way the research of several electrical components that can be easily integrated into packaging, such as EHD.

Since paper itself is not a piezoelectric material, there is the need to deposit another material that has this property to provide the EHD's potential energy generation. Additionally, in this type of electrical devices, it is of a huge importance to use materials that are sustainable, abundant, and low-cost such as ZnO, which draws its attention due to its piezoelectric properties, responsible for the energy generation. An automatic film applicator was utilized as the printing method, applying piezoelectric structures such as ZnO rods, mixed within a cellulose-based matrix to ensure the production of robust EHDs, while maintaining the concern for the use of environmentally friendly and recyclable materials.

The ZnO rods were produced by hydrothermal synthesis assisted by microwave irradiation. Subsequently, these structures were mixed in the matrix, and applied afterwards to the paper to functionalize it. The ZnO rods were morphologically and structurally characterised with scanning electron microscopy (SEM) and X-ray diffraction (XRD) techniques, and the EHD was characterised with the SEM technique. The performance of the functionalized paper for energy harvesting was optimized by varying the EHD's structure and its composition.

#### Outputs

The work performed in this dissertation project resulted in an oral and poster presentation in the following international conference, RSC Chemical Nanoscience and Nanotechnology Early Career Researcher Virtual Poster Meeting, on the 20th of June 2022, inserted in the area of Energy. In this conference a brief introduction of the context and the methods was presented summarizing the work done. This participation on the international conference brought numerous great aspects, such as the divulgation of this innovational scientific work, receiving feed-back from colleagues and fellow scientists, and a chance to practise the exposure of this work.

Here is the previous mentioned output:

#### Posters:

Tiago Silva\*, Andreia dos Santos, Ana Rovisco, Cristina Gaspar, Elvira Fortunato, Rodrigo Martins, Pedro Barquinha and Luis Pereira, Sustainable Energy Harvesting Paper for Interactive Smart Packaging, RSC Chemical Nanoscience and Nanotechnology Early Career Researcher Virtual Poster Meeting, 20th June 2022.

Additionally, the work presented in this thesis is being prepared in the format of a manuscript to be submitted to a scientific journal.

# 1 Introduction

# 1.1 Smart Packaging

Over the years, the importance of packaging all kind of products has been increasing, whether because the product is fragile, food-related, or for the protection of its integrity, so that the product can be safely distributed from the place of production to the consumer, thus avoiding product waste, deterioration, and damage [1]. In most cases, the consumer buys the product and not the packaging itself, except in cases where the purchase is motivated, for example, by advertising or its aesthetic aspect [1]. The packaging, after being used by the consumer, can easily become a frustration, for example in the way that it can be difficult to open, to reseal, fail to clearly show the written information on the label, and even problematic to empty completely [1]. The term "smart packaging" was defined as packaging that serves a purpose that goes beyond the traditional functions of storage, protection, and product information [2]. This term covers several aspects, from the design to the use of smart materials and the incorporation of mechanical and/or electronic sensors, incorporated into the packaging or its surface [1].

To satisfy consumers looking for more information, better quality of goods, and appealing packages, Smart Packaging solutions were developed. These can be divided into two distinct branches: Active, which act directly on the products in order to delay their deterioration, for example the films that absorb oxygen, such as sponges inside meat packages [3], [4]; and Intelligent, which monitor the quality of the product [1], for example packages that have sensors to monitor the levels of gases or pH, and communicate this information with the user, either by colorimetric indicators or by quick response codes (QR) [1], radio frequency identification (RFID) [2], or others.

Interactive Packaging, which is a subsection of Intelligent Packaging, relates to packages whose goal is not to monitor the package product but to interact with the consumer through functional and amusing elements, as a marketing strategy or creating a link to benefit the product sales [1]. These elements can be: printed labels, wireless communication chips (RFID) [2], quick response codes (QR), light [5] or sound systems. These elements frequently require a power source, whether using batteries, wireless power, light or heat to power electrical devices or sensors [6]. However, the use of batteries [1], [5] should be avoided, so that these packages do not become a problem at the time of disposal. An EHD made of eco-friendly materials can

be used to tackle this issue, allowing, for instance, the packaging to be recycled and reused rather than being thrown away after only one use or after a brief time life.

It is common for EHDs to have both a piezoelectric effect and a triboelectric effect in a single device in order to maximize the energy output of the device [7]–[13][9].

# 1.2 Energy Harvesters Devices

A device known as an energy harvester transforms a certain form of energy into electrical energy for storage or to be used in a circuit, being important to note that a generator does not produce any energy, it just transforms it [14]. This transformation can have as input various types of energy, for example mechanical, the most widely distributed resource, which can take several forms, such as steam, combustion gases, wind, water, or even physical impacts [14]. Amongst other types of energy, one can highlight the solar, wind and magnetic ones [14]. Every generator, and the energy input associated, presents advantages and disadvantages. For instance, on the one hand, solar and wind generators, have an energy source that is renewable and non-polluting, but on the other hand, its installation is costly and the technology is highly dependent on meteorological conditions, as well as the area where the generators are installed [15]. Between other several types of mechanical generators, coal burning, for example, has several problems associated with cost, maintenance, complexity and the size of infrastructures needed, or even worse, it is not environmentally friendly at all, despite the substantial amounts of energy produced [16]. Micro and nano-scale mechanical generators draw attention due to their dimensions, low-cost, and ability to transform various types of energy into electrical energy, being capable of powering a device or store the energy for later use [11].

In 2001, Glynne-Jones et al. [17] proposed a micro piezoelectric generator powered by vibrations. Two years later, in 2003, fibre-based piezoelectric materials for energy use were investigated by Churchill's group [18]. The results showed that, although being small, these piezoelectric structures could produce enough energy for wireless transmission [18]. In 2006 a new piezoelectric nanogenerator (PENG) of ZnO was suggested by Prof. Zhong Lin Wang and colleagues [12], [19]. Following the 2006 demonstration of the first nanogenerators (NG) [19], a number of projects emerged that added variation to nanostructures and architectures while efficiently converting mechanical energy into electrical energy, primarily using the piezoelectric [13] and triboelectric effects [12], [20]–[22]. Recently, NGs with an added mechanical flexibility function have been developed, and they were promising in offering power generation solutions for compliant and flexible electronic devices [12], [13], [23]–[26]. An exponential increase in the number of publications related to triboelectric nanogenerators (TENG) was observed from just 8 in 2012 to 400 in 2017 [27].

# 1.3 Piezoelectricity

Piezoelectricity occurs from the electromechanical linear interaction between the mechanical state and the electrical state of crystals without a centre of symmetry [28]. This phenomenon is present when a mechanical deformation of the piezoelectric material produces a proportional change in its polarization, inducing the appearance of electrical charges on opposite faces of the material [28]. This process can also happen in the opposite direction, by applying voltage to the material to induce its deformation [28]. The dimensions of piezoelectric materials can be reduced in a way that they can be processed into nanoscale devices while maintaining their functional properties. A PENG converts mechanical energy into electrical energy and has the potential to operate in a wide frequency and motion range [12]. The working mechanism of PENGs can be described as a transient flow of electrons guided by a piezoelectric potential [29], [30]. Figure 1.1 illustrates the working mechanism of a PENG.

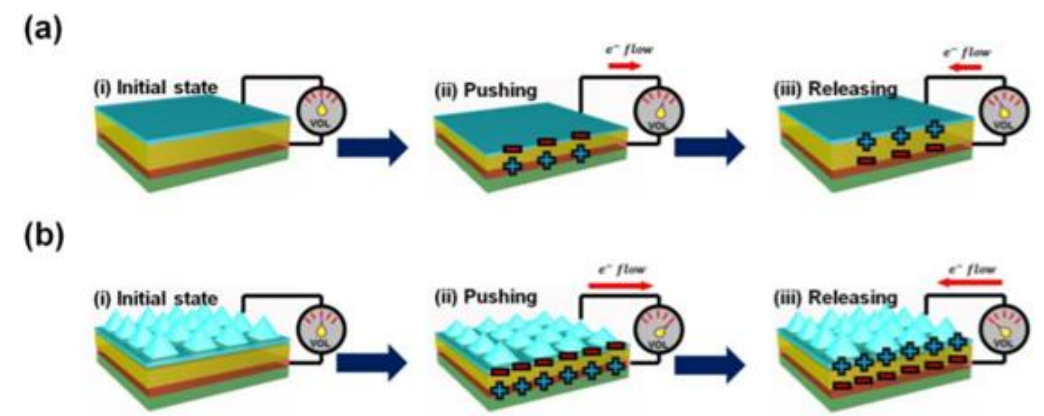


Figure 1.1 - Working mechanism of the piezoelectric devices under external forces, compression, and decompression, in **(a)** a device without surface structures and in **(b)** a device with pyramidal shapes on its surface.

Image of supplementary reference material [31].

When piezoelectric structures are distorted under mechanical action, (direct impact or flexing), wind, human movement, rolling tires, sound waves or even vibrations, from machines, the charge separation process develops a piezoelectric potential capable of inducing an electric current that can power devices with low energy consumption [11], [12], [32]. One of the main applications of NGs are self-powered systems, which capture energy from the environment and convert it into electricity to achieve maintenance-free and autonomous operation [12].

# 1.4 Triboelectricity

The triboelectric effect is omnipresent in our daily lives and results from the contact of two different materials [27]. It is usually seen as a negative aspect in the industry as it can induce electrostatic charges that can lead to ignition, dust explosions, dielectric breakdown, and even electronic damage [25]. From an energy point of view, these electrostatic charges

represent a device with energy capacity when the two triboelectric surfaces are separated. Associating this triboelectric effect with electrostatic induction, the TENG was first invented by the group of Zhong Lin Wang in 2012 to efficiently capture the ambient mechanical energy that, despite being omnipresent per system, is not usually used [27]. More specifically, triboelectrification provides static polarized charges on the surfaces of materials in contact, while electrostatic induction leads to the transformation of mechanical energy into electricity through the electrical potential change induced by mechanically agitated separation [27]. In the last 6 years, the concept of TENG has expanded into different working modes to allow applications in different scenarios [22], [33]–[36], such as mechanical vibrations, human movement, wind, and ocean waves (blue energy) [22], [27], [37].

The four operating modes of TENG, illustrated in Figure 1.2, were proposed in 2012, depending on the change in polarization direction and electronic configuration, being the following: vertical contact-separation mode, lateral-sliding mode, single-electrode mode, and freestanding triboelectric-layer mode [27].

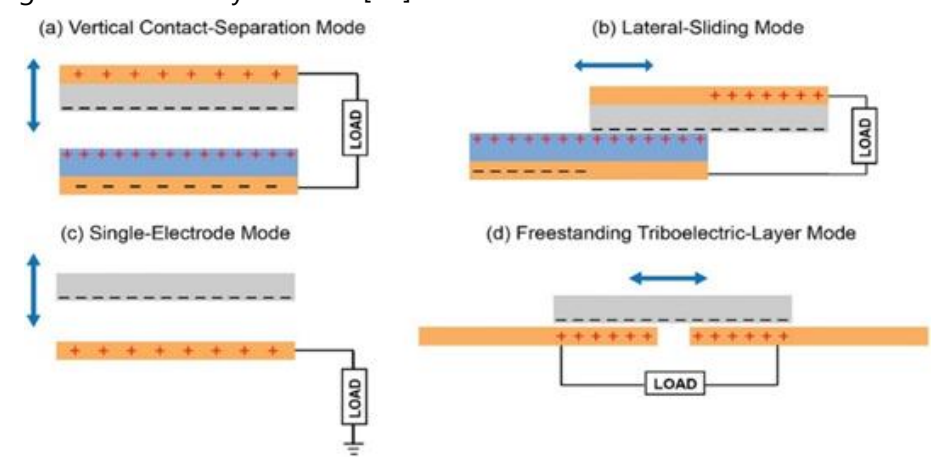


Figure 1.2 - The four different modes of operation of the TENG. In **a)** the vertical contact-separation mode; **b)** lateral-sliding mode; **c)** single-electrode mode; and in **d)** freestanding triboelectric-layer mode. Image adapted from [27].

#### 1.5 Cellulose

Cellulose is the most abundant natural polymer resource on earth, which has sustainable qualities such as being environmentally friendly, renewable, biodegradable, inexpensive, and having excellent biocompatibility [11]. Recently, among the immense applications of cellulose, applications focused on energy use have been studied [11], [38]. The high crystallinity and abundance of polar hydroxyl groups, accompanied by the arrangement of asymmetric monoclinic and triclinic crystals, endows cellulose with numerous asymmetric dipoles with piezoelectric activity and a strong electron donation capacity, being a promising potential for piezoelectric and triboelectric effects [11]. Additionally, cellulose can be used as a substrate for

devices with the purpose of energy harvesting [39], or as a matrix for a composite with piezoelectric structures for the functionalization of other substrates [40].

#### 1.6 Piezoelectric Materials

The choice of piezoelectric materials for an energy-harvesting application has a major impact on device functionality and performance. These generators are currently made at the micro and nanoscale from a variety of materials. Some examples of materials with piezoelectric effects are piezoelectric ceramics, such as barium titanate (BaTiO<sub>3</sub>) [41], [42] and lead zirconate titanate (PZT) [32], [43], being the latter the most used. There are also piezoelectric polymers such as polyvinylidene difluoride (PVDF) [32], [44]-[46] and polyamide (PA) [11], [47], [48], or even metallic oxides such as ZnO [7], [11], [32], and ZnSnO3 [8]. Each of these materials has the ability to convert mechanical energy into electrical energy and the other way around [12]. PZT has been widely used since the start of the twenty-first century, but due to its brittleness, the maximum stress that may be applied without causing fracture is constrained [12]. ZnO nanostructures have attracted attention as functional elements for NGs due to their advantages such as high transparency, lead-free chemical composition, the ease of obtaining different nanostructures, chemical stability, the potential to combine their semiconductor and piezoelectric properties [10], [18], [49], [50], and being free of critical raw materials, unlike PZT and BaTiO<sub>3</sub> [51]. A cellulose-based PENG normally consists of three parts: a piezoelectric active intermediate layer, a pair of conductive electrodes and an outer insulating layer [11]. This outer layer gives the PENG sufficient mechanical strength and recoverability [11].

## 1.7 Triboelectric Materials

Practically all known materials have this triboelectric effect, from metals to silk, wood, among others [28]. However, a material's ability to gain or lose electrons depends on its polarity, and the greater the difference in polarity of the materials that make up to TENG, the more charges will be induced on the surface of each material [52], [53]. Usually, one material with a tendency to gain electrons is combined with another that tends to lose them. Adding to this choice of materials for the TENG, it is also necessary to take into account the morphology of their contact surface, which can be altered by physical techniques, for example through the creation of micro or nano patterns of pyramids [52], in order to obtain better output voltages. The most used materials with triboelectric effect are polydimethylsiloxane (PDMS), which is low-cost [32], [48], [54], [55], PVDF [56]–[58], polytetrafluoroethylene (PTFE) [59], PA [60], etc. Even raindrops can be used to harvest electrical energy [61]. There are countless ways to combine two materials with various triboelectric polarities to create a triboelectric device [40].

# MATERIALS AND METHODS

This chapter reviews the materials and the experimental techniques explored throughout this thesis. Firstly, the materials needed to produce the piezoelectric and triboelectric EHD are described, followed by the methods necessary to produce these EHD and how to characterize them electrically.

#### 2.1 Materials

First, the synthesis of ZnO and of the three composite matrices, PDMS, CMC and EC, are described here, along with the two substrates (papers) used: Navigator and Whatman.

### 2.1.1 Zinc Oxide Rods Synthesis

The ZnO rods were obtained by hydrothermal synthesis assisted by microwave irradiation, as described in [7]. The synthesis started with 3.3 q of zinc acetate dihydrate, CAS: 5970-45-6, (ACS, 98-101%, Fisher Scientific) dissolved in 30 mL of deionized water, with the help of a magnetic stirrer. Afterwards 9.6 g of sodium hydroxide, CAS: 1310-73-2, (98.0-100.5%, Honeywell FlukaTM) were added to the preceding solution. In order to create the surfactant solution, 0.045 g of sodium lauryl sulfate, CAS:151-21-3, (SLS, 95%, extra pure, Scharlau) were combined with 150 mL of deionized water. Upon complete dissolution of both solutions, 6 mL from the first solution, 15 mL from the surfactant solution, and 30 mL of 2-ethoxyethanol, CAS: 110-80-5, (reagent grade 99%, Honeywell) were mixed and stirred. The resulting solution was poured into three Teflon® vessels, each one holding 17 mL of the final solution. These vessels were placed in a microwave digestion system (CEM-MarsOne, CEM) to be heated at 110 °C for 40 min, under a power of 600 W. After that, the vessels were cooled down to room temperature and the ZnO rods were then cleaned through repeated centrifugation at 3000 rpm for 3 min with 2-propanol, CAS: 67-63-0, (Labchem Laborspirit) and deionized water, intercalating for 3 times each. Finally, the rods were dried inside a desiccator (VACUO-TEMP, J. P. Selecta) at 85 °C for 5 h in a vacuum atmospheric pressure.

#### 2.1.2 PDMS

PDMS was obtained by a simple process, as described in previous works [7], [8], to create the piezoelectric and triboelectric EHDs. It was obtained by mixing an elastomer (CAS: 63148-62-9, Dow Corning) with a corresponding curing agent (Sylgard 184, Dow Corning) in a weight

ratio of 10:1, respectively. The mixture was manually stirred, creating bubbles that were removed afterwards in a desiccator for 30 min, before being ready to be used.

#### 2.1.3 CMC and EC

For the production of the EHDs with CMC as matrix, a solution was made with a 3 wt.% ratio of sodium CMC, CAS: 9004-32-4, (Sigma-Aldrich Chemistry) to deionized water, with a magnetic stirring for 24 h.

On the other hand, to produce EHDs with EC as matrix, a solution was made with a 5 wt.% ratio of EC, CAS: 9004-57-3, (Sigma-Aldrich Chemistry) to ethanol, CAS: 64-17-5, (96%, Labchem Laborspirit) and diacetone alcohol (DAA), CAS: 123-42-2, (Sigma-Aldrich Chemistry) in equal parts, with a magnetic stirring for 24 h.

#### 2.1.4 ZnO coatings

To produce the EHDs, ZnO rods were mixed with the PDMS elastomer, CMC, or EC in a ratio of 25 %, in weight, which was already optimized in [1], and ethyl acetate, CAS: 141-78-5, (Fluka Chemika, Sigma-Aldrich Chemistry GmbH) at a volume that promoted the mixing of the elastomer and rods, staying at least 24 h mixing with a magnetic stirrer. Only after most of the solvent volume had been evaporated, the curing agent was added in a weight ratio to elastomer of 1:10, and thoroughly mixed and desiccated before use.

#### 2.1.5 Substrates

#### 2.1.5.1 Polyethylene terephthalate (PET) and an indium tin oxide (ITO) - PET/ITO

Commercial substrates of polyethylene terephthalate (PET) with an indium tin oxide (ITO) thin film deposited on top, PET/ITO (Kintec Company), were used with the purpose of compressing the composite on both sides, and also as a result of ITO's conductivity, as an electrode in both sides.

#### 2.1.5.2 Papers: Navigator & Whatman

Standard paper Navigator (120 g/m<sup>2</sup>, The Navigator Company) and Whatman<sup>TM</sup> (grade 1, Cytiva) were used to replace the PDMS matrix, used in [7], [8], the first being a less porous paper with a whitening treatment, and the second being a more porous paper.

#### 2.2 Methods

## 2.2.1 Screen Printing

The process through which the electrodes were applied to the substrates was screen printing and the illustrative scheme of this custom-made system is in Figure A.1.

The screen (120T) with the pattern that was most appropriate to the application of the silver (Ag) electrode was selected from, a 1.7 cm square or a 2 cm by 4 cm rectangle, depending on the geometry of the cut substrate, considering the limitation of the slot for the EHD on the bending machine that is 3.5 cm. With the help of the squeegee in an approximately 45° angle to the screen and pressing with a constant down force relatively to the screen, conductive silver, (Coates Screen Inks GmbH) was applied to several different EHDs' structures, with drying times of 5 min at 120 °C in a hot plate onto both sides of the substrate, one at a time. The electrodes on both sides needed to be off-centred to avoid a short circuit.

## 2.2.2 Automatic Film Applicator or Coater

The coatings for the EHDs were made with a coater (K Control Coater, RK Print Coat Instruments) using a wound metal bar (K101 Bar No. 8 Blue/100 Micron) that produced films with 100 µm thickness with the set speed of 2 (approximately 0.6 m/min). The setup was straight forward and involved taping the substrate's corners with duct tape, from the side that the bar was moving and on the lateral sides, while applying the substrate coating, only on one side of the substrate.

#### 2.2.3 Electrical Characterization

A home-made bending machine with a linear motor, Figure A.2, was used to deliver a mechanical stimulus with a frequency of 1 push per second, with an impact area of 0.3 cm<sup>2</sup> on the EHD. Using a commercial force sensing resistor (Ref. SEN05003, Interlink Electronics) the estimated force applied on the produced EHDs was of 9 N. The final output voltage of the EHDs was collected by a digital oscilloscope (TBS1000C, Tektronix), providing sufficiently high resolution for registering the exact peak levels of the generated waveform. Electric probes (10x voltage probe, TPP0100, Tektronix) were used to connect the oscilloscope to the device's electrodes.

## 2.2.4 Morphological and Structural Characterization

The morphological and structural characteristics of the ZnO structures and the EHDs were studied by a scanning electron microscope (SEM Hitachi TM3030Plus). Additionally, diffractograms of the ZnO rods were collected by X-ray diffraction, XRD, (using a PANalytical's X'Pert PRO MRD), to determine the purity and crystallinity of the ZnO rods. More information and specifications of the experiments made are in appendix A.3 and A.4.

# **RESULTS AND DISCUSSION**

This chapter describes the characterization of the ZnO rods synthesised, meticulously studies of the characterization of the EHDs produced in this work, and presents, explains, and thoroughly analyses the global results collected during this thesis.

## 3.1 Characterization of the zinc oxide rods

Several syntheses of ZnO rods were made during the period of this work and both XRD and SEM analyse were conducted to thoroughly characterize the ZnO rods, namely the crystallinity, morphology, and the average size of the rods.

## 3.1.1 Scanning electron microscopy (SEM) of the ZnO rods

The observation of the morphology of the rods was performed using a SEM. Figure 3.1 presents two neat images obtained of the ZnO rods synthesised, only varying the magnification utilized. When observing the high magnification image, it is possible to see that the ZnO rods are well separated, and that the length and diameter sizes of the rods have low dispersion. Observing the low magnification image, it is noticeable that besides the expected separated rods, some of them are aggregated in a flower shape ZnO structure [62], [63].

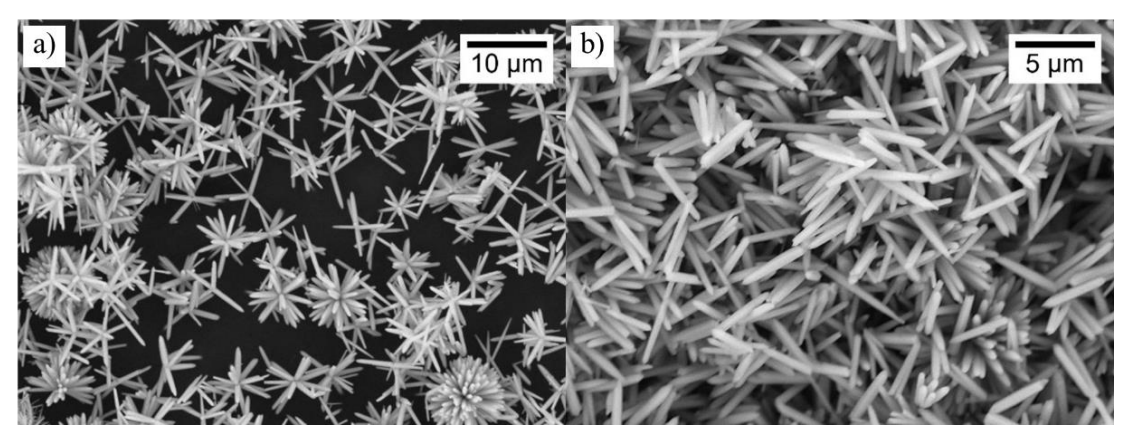


Figure 3.1 - SEM images of the ZnO rods synthesised, with different magnifications: a) ×2500 and b) ×5000.

Over time, these newly created rods deposit on the surfaces of previously formed crystalline rods, resulting in an ordered array that looks like a flower shaped ZnO structure [63]. This development occurs naturally and is thermodynamical motivated, leaving up to a large flower shape ZnO structure, because this shape is more energetically stable when compared to the loose rods, proving that the surface molecules of the particles are not as energetically stable as the rods in the core [63].

#### 3.1.2 Rods Dimensions

Size regularity is an important index to assess the quality of nanomaterials. High uniformity dimensions can greatly improve the reliability and reproducibility of EHDs made with such nanomaterials. Therefore, the size uniformity of the synthesised rods of ZnO was investigated by studying the distribution of both their length and diameter. Using the software ImageJ (more details in Appendix A.3) the measurements for the length and diameter of the ZnO rods were made. Figure 3.2 a) and b) shows the distributions of the length and the diameter, respectively, of the ZnO rods made with a frequency of 150, n = 150, including three different syntheses, 50 measurements from each, between several SEM images, of the process done and explained in the subsection 2.1.1.

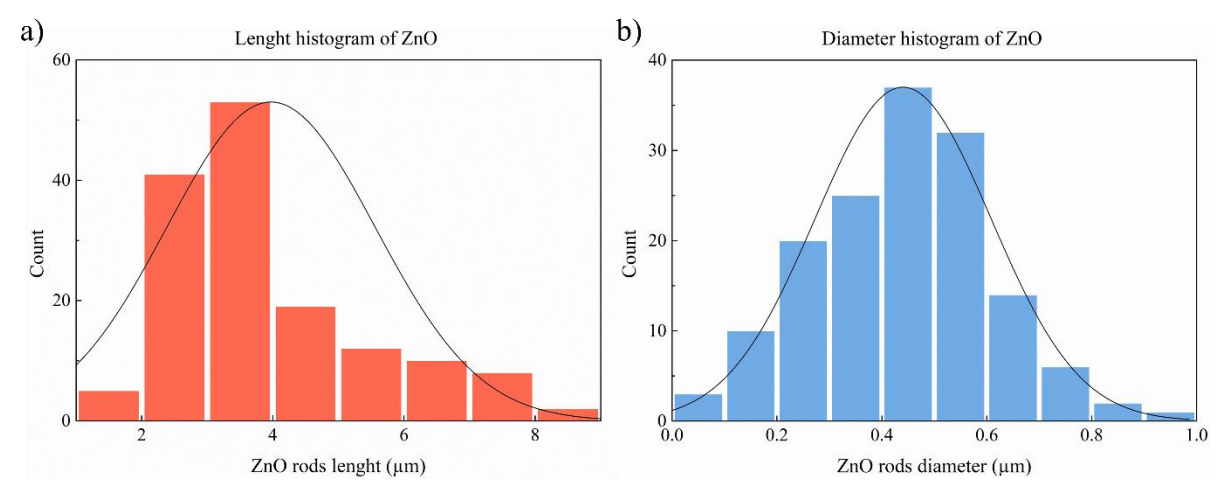


Figure 3.2 - Histograms, with a frequency of n = 150, showing **a)** the length distribution and **b)** the diameter distribution of the ZnO rods produced in different syntheses (second, eighth and ninth syntheses), for effects of repeatability of the synthesis.

It can be seen in Figure 3.2 **a)** that the length of the ZnO rods ranges from 1  $\mu$ m to 9  $\mu$ m. The black solid line is the corresponding Gaussian line-fitting, and it follows a reasonable normal distribution. It shows that the average length of the ZnO analysed is of 3.97  $\mu$ m with a standard deviation of 1.59  $\mu$ m.

Alike the previous length histogram, the diameter distribution histogram is shown in Figure 3.2 b), where the diameter of most of the produced ZnO rods is located between 100 nm and 1000 nm. The black solid line corresponds again to the Gaussian line-fitting, and it follows a reasonable normal distribution. It is shown that the average diameter of the ZnO rods studied is 440 nm with a standard deviation of 168 nm. Overall, the ZnO rods follow a good normal distribution and are rather uniform in dimension. The fact that the rods dimensions are kept uniform, synthesis after synthesis, proves the reproducibility of the method.

The aspect ratio of the ZnO rods synthesised was calculated with the aspect ratio formula, diving the average length of the ZnO rods by the average diameter of the ZnO rods, resulting on an aspect ratio of 9.

## 3.1.3 X-ray diffraction (XRD) studies of ZnO rods

Figure 3.3 shows the XRD diffractogram of the ZnO rods synthesised. The observed peaks match the ones specified on the identification card of ZnO (ICDD card #36-1451). The peaks are observed at 20 values of 31.8°, 34.4°, 36.3°, 47.5°, 56.6°, 62.8°, 66.4°, 68.0°, 69.1°, 72.6°, 76.9° corresponding to the following lattice planes (100), (002), (101), (102), (110), (103), (200), (112), (201), (004), (202).

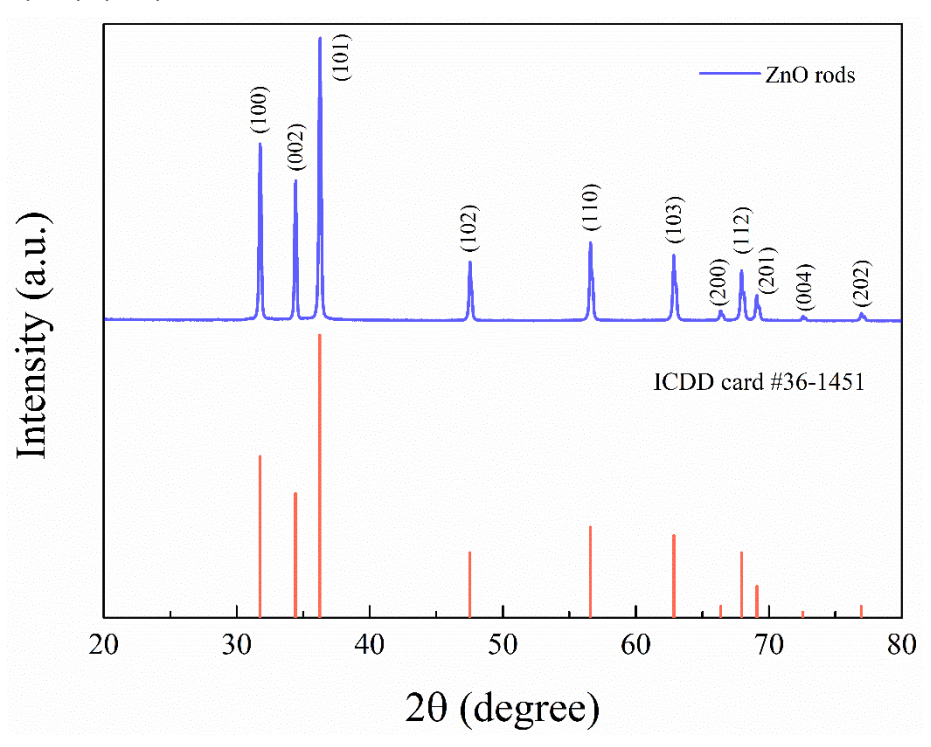


Figure 3.3 - XRD diffractogram of ZnO rods. The identification of ZnO was made following ICDD card #36-1451.

With such an exceptional matching of the peaks of the diffractogram to the specified ones on the identification card, it can be concluded that the ZnO synthesised shows an elevated level of purity and phase structure of the powder, without any impurities being observed.

## 3.2 Energy Harvester EHDs

## 3.2.1 Topographical Characterization of Embedded Substrates

Figure 3.4 contains several SEM images from a top viewpoint, in order to analyse the surface topography of the possible combinations between two substrates, Whatman (left) and Navigator (right), and a control (only paper) substrate plus three matrices, CMC, EC and PDMS,

from top to bottom. The same composite matrix in two distinct substrates is shown in side-by-side images, always with the same magnification (×200) for comparison purposes.

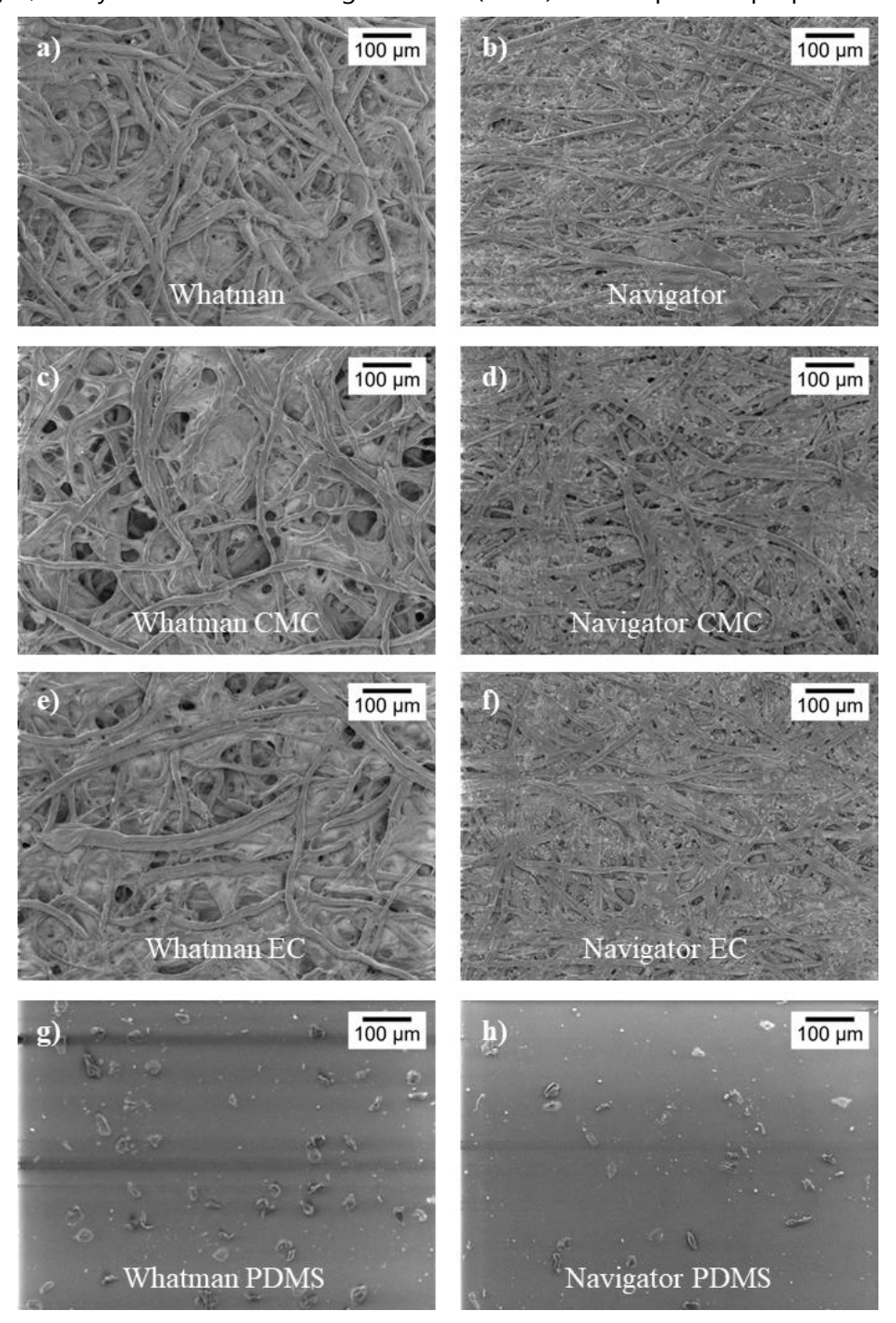


Figure 3.4 - SEM images from a top viewpoint of several embedded substrates produced. Vertically, the substrates are Whatman (on the left) and Navigator (on the right). Horizontally there is a control (only paper) followed by 3 matrices, CMC, EC and PDMS. Substrates: a) Whatman, b) Navigator, c) Whatman with CMC, d) Navigator with CMC, e) Whatman with EC, f) Navigator with EC, g) Whatman with PDMS, and h) Navigator with PDMS.

As a starting point, acting as control samples for the remaining embedded substrates, two substrates were studied, Whatman in Figure 3.4 a) and Navigator in Figure 3.4 b). Being

Whatman the most porous paper between the two, the figure shows entangled fibers that have more space between them, being slightly looser and, as a consequence, more permeable.

A perception of depth can be visible, and the fibers themselves are more fibrous that the ones visible in Navigator substrate, Figure 3.4 b), where some evenly spread dots can be seen across the surface of the fibers. In fact, during production this paper receives a specific treatment, where calcium carbonate is added, working as a filler covering the pores, whitening the paper, and also smoothing the surface [64]. Consequently, the fibers are more compacted, leaving less space between them, which reflects on the paper being less porous and, as a result of its porosity, it is a less permeable paper when compared to Whatman. In Figure 3.4 c) and Figure 3.4 d), only the matrix CMC was applied to both substrates with an automatic film applicator. After deposition, the CMC started straight way to be embedded in the paper, followed by drying 24 h at room temperature with duct tape in all sides to avoid wrinkling, in order for the embedded substrates to be practically flat and facilitate the remaining EHD production steps. The fibers on the surface were reasonably identical to the control ones, with more connections between the fibers due to the dried CMC. Similarly to the previous two images, in Figure 3.4 e) and Figure 3.4 f), only EC was applied to both substrates using the same method and drying procedure. Visually the difference between the fibers embedded with CMC or with EC is narrow, but it can be noticed that both substrates got more compacted when embedded in EC when compared to the CMC in the same conditions. Taking into account the significant difference in porosity of both papers, the celluloses were embedded slightly differently, they were well embedded in Whatman and lightly less so in Navigator. Finally, concerning the last two SEM images, Figure 3.4 g) and Figure 3.4 h), the PDMS matrix had more viscosity than the previous matrices, and was also applied with the same method, but dried in the oven at 75°C during 1 h for the polymer to cure. PDMS was significantly less embedded on both substrates compared to the celluloses. Both SEM images were taken from the side where PDMS had been applied, because while holding them in hand, one side had clearly a shinier aspect. Visually almost no differences can be seen between both surfaces of the different substrates, but some imperfections, such as dust that got caught in some part of the process and perhaps loose fibers or tips of them, resulting from the drying process, can be observed.

## 3.2.2 Dimensional Characterization of Embedded Substrates

Figure 3.5 shows the cross-section SEM images of several embedded substrates, to examine and respectively determine their thickness for comparison purposes. Similar to Figure 3.4, all the possible combinations are shown starting with the two substrates, Whatman (left) and Navigator (right), and a control substrate plus three matrices, CMC, EC and PDMS, from

top to bottom. The same composite matrix in two distinct substrates is shown in side-by-side images, always with the same magnification (×300) for comparison purposes.

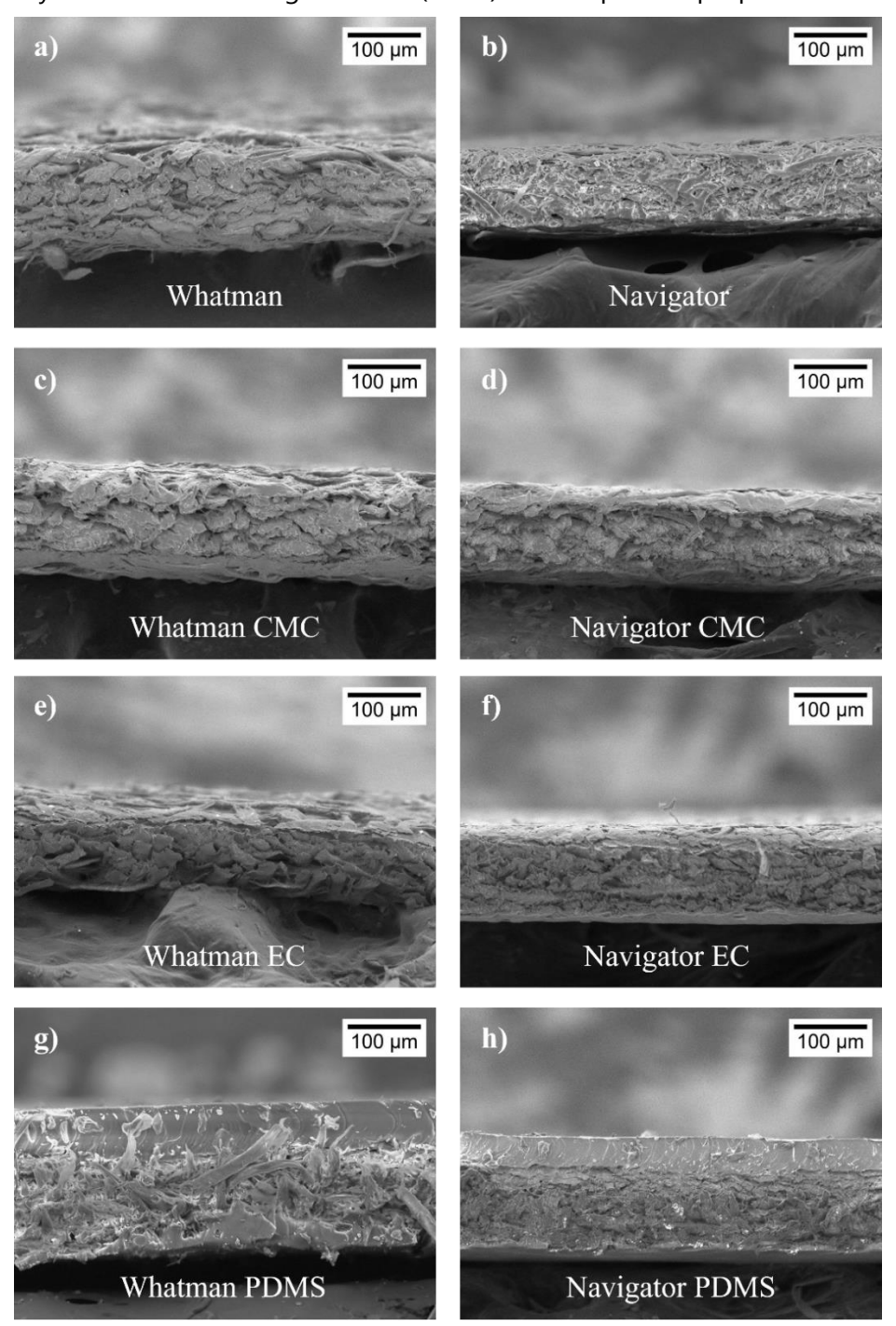


Figure 3.5 - SEM images from a cross section point of view of several embedded substrates produced. Vertically, the substrates are Whatman (on the left) and Navigator (on the right). Horizontally there is a control followed by 3 matrices, CMC, EC and PDMS. Substrates: a) Whatman, b) Navigator, c) Whatman with CMC, d) Navigator with CMC, e) Whatman with EC, f) Navigator with EC, g) Whatman with PDMS, and h) Navigator with PDMS.

Firstly, looking at the control samples for the remaining embedded substrates, both substrates, Whatman in Figure 3.5 a) and Navigator in Figure 3.5 b), were studied.

Observing Figure 3.5 a) the substrate has more loose fibers or fibers tips, coming out of the substrates surface, and also more pores, when compared to the substrate in Figure 3.5 b) where the substrate is more compacted and less porous. In images c) and e) in Figure 3.5, where respectively CMC and EC were added to the substrate Whatman, this issue of loose fibers is absent, because of the embedding and drying of the celluloses on the substrate, where the fibers seems to be more compacted and there is significantly less loose fibers on the surfaces. The same effect of the fibers being more compacted is less visible in image d) and f) in Figure 3.5, with CMC and EC on Navigator substrate. Between both celluloses visually there is no difference on the look of the cross section in both substrates. On the last two images in Figure 3.5, g) and h), where the matrix added was PDMS on both substrates, the side where the film was applied is quite easy to tell apart, on top. Although a consistent PDMS thick layer can be seen on the top of both substrates, the matrix is not very deeply embedded in the substrate. As a consequence to this, these two types of embedded substrates produced, Whatman with PDMS and Navigator with PDMS, have the most heterogeneity between the embedded substrates surfaces, when compared to the previous embedded substrates analysed. Keeping in mind that both embedded substrates sides are meant to have a silver electrode.

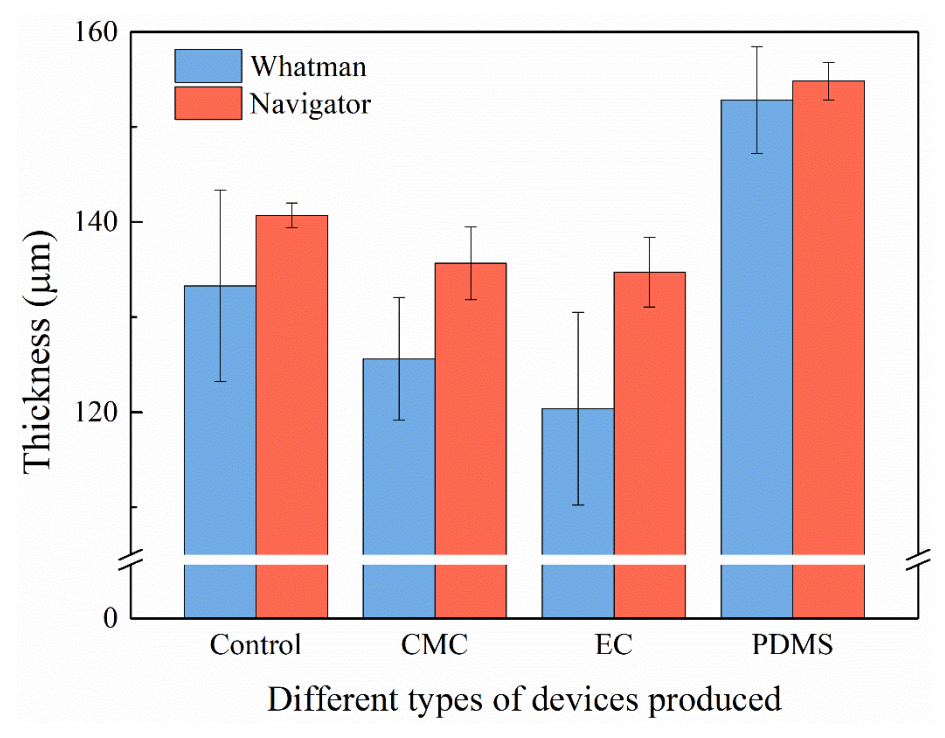


Figure 3.6 - Column chart showing the thickness of various embedded substrates produced. The substrates are separated by colours, in blue Whatman and in red Navigator. The paired columns have the control sample followed by 3 matrices, CMC, EC and PDMS (from left to right).

Figure 3.6 consists of a bar chart that displays the average thickness value and respective standard deviation, for each embedded substrates produced, obtained by making 10

measurements in each image. The substrates are separated by colours, Whatman in blue and Navigator in red, and on the x-axis are the paired columns with the control sample followed by the 3 matrices: CMC, EC and PDMS, from left to right.

By examining the columns in Figure 3.6, a substantial difference can be seen between the values of the standard deviations for the average thickness of the Navigator embedded substrates compared to the Whatman ones, with Navigator having an average error value of 2 %, against the 6 % seen in the Whatman embedded substrates presented. This indicates that the Navigator's thickness is considerably more constant than the thickness of the Whatman, in all produced substrates (control and three matrices). Therefore, the Navigator paper has a higher finished quality then the Whatman paper. A subtle decrease on the thickness from the control substrate and the substrates with embedded cellulose can be seen. In opposite, a higher increase of the thickness is seen from the control substrate to the ones that have PDMS as matrix.

Starting with the control samples, the substrate Whatman in Figure 3.5 **a)**, has an average thickness and respective standard deviation of (133  $\pm$  10)  $\mu$ m, being lower when compared to the substrate Navigator in Figure 3.5 **b)**, which has an average thickness and respective standard deviation of (141  $\pm$  2)  $\mu$ m. Putting this in comparison with the substrates embedded with PDMS, Whatman with PDMS in Figure 3.5 **g)**, has an average thickness and respective standard deviation of (153  $\pm$  6)  $\mu$ m, presenting again a lower thickness then the Navigator with PDMS in Figure 3.5 **h)**, which has an average thickness and respective deviation of (155  $\pm$  2)  $\mu$ m.

The major difference on the average thickness value was between control substrates and the ones with PDMS as matrix. After the PDMS deposition, the substrate Whatman had an additional 20  $\mu$ m on the average thickness, while the substrate Navigator had an added 14  $\mu$ m. A thicker EHD embedded substrate will have different impacts that will affect some properties, for example the piezoelectric capability of the EHD.

The major decrease in thickness was seen in the substrate Whatman, decreasing 8  $\mu$ m when CMC was applied and 13  $\mu$ m when EC was applied, based on both thickness averages, comparing the measures with the control sample. In the other hand, when CMC was applied to the substrate Navigator, the thickness decreased in 5  $\mu$ m and when EC was applied, the thickness decreased 6  $\mu$ m. This happens because the substrate Whatman is less compact than the substrate Navigator by nature, and when either CMC or EC was applied on one side of the substrate, it was embedded in a way that the fibers lightly contracted and got more packed between them, decreasing the thickness of the embedded substrate. The embedded substrates where the matrix is PDMS, are thicker because this matrix gets less embedded in the papers when compared to the celluloses, creating an easily distinguishable layer.

Given that the standard deviations of the measurements of the embedded substrates thickness are all below 10 %, it can be concluded that the method used to deposit the films on the substrate is highly reproducible after deposition of either of the three matrices.

## 3.2.3 Opacity and Flexibility of the EHDs

Figure 3.7 presents three different types of EHDs produced, being the following ones, matrices between the PET/ITO electrodes, represented in Figure 3.7 a) and b), matrices with ZnO rods mixed embedded in the substrates between PET/ITO electrodes showed in Figure 3.7 c) and d), and lastly matrices with ZnO rods mixed embedded in the substrates with Ag electrodes in Figure 3.7 e) and f). A batch of EHDs was produced within the same conditions to the ones in previous works [8], shown in Figure 3.7 a), clearly transparent, opposing to the basically opaques EHDs shown in Figure 3.7 c) and e), being e) a bit less opaque then c). All EHDs produced in this work, except for the control ones with only PDMS, CMC or EC as the matrix between the electrodes, were quite opaque. This happens firstly due to the fact that the substrates used were paper, and paper alone is opaquer. Secondly, although the matrices here employed, PDMS, CMC and EC, are transparent, when mixed with the ZnO rods, the matrices gain a white colour, which turns them opaque.

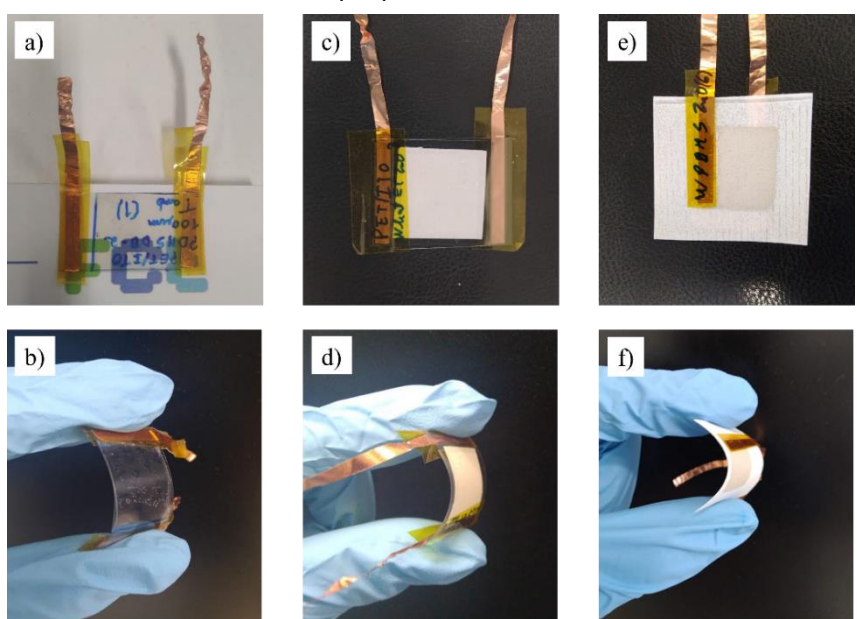


Figure 3.7 - Six photographs, to contrast the transparency in **a**) and opaqueness, in **c**) and **e**), of the EHD produced, and showing the flexibility associated with each one, in **b**), **d**) and **f**). Comparing the EHD constructed in the previous work [8], with the ones in the present investigation. EHDs displayed: **a**) and **b**), PDMS between the PET/ITO electrodes, **c**) and **d**), substrate Whatman, embedded with EC mixed with ZnO rods, between PET/ITO electrodes and lastly, **e**) and **f**), substrate Whatman, embedded with PDMS mixed with ZnO rods, with Ag electrodes.

Photographs **b**), **d**) and **f**) in Figure 3.7, show the high flexibility of the EHDs produced in this dissertation, which is an indispensable factor for the main application in Interactive Smart

Packaging. In Figure 3.7 f), a remarkably bendable EHD is displayed with printed Ag electrodes, demonstrating higher flexibility, when compared to EHDs build with PET/ITO electrodes, in Figure 3.7 b) and d).

#### 3.3 Electrical Characterization of the EHDs

The major characterization method of this dissertation was the electrical one, which was performed to all produced EHDs with the purpose of getting the best possible output voltage of each sample, which is simply the peak-to-peak value. Taking this into consideration, all conditions involved around the electrical characterization were required to be kept constant throughout the measurements. The impact force was maintained constant during characterizations tests done to all EHDs to have an even comparison, 9 N on each impact with a frequency of one push per second. In EHDs with Ag electrodes the impact needed to occur on the area of the electrode itself. The voltage generated from the EHD depends on the area of contact of the bending machine impact, which was maintained constant at a value of 0.3 cm<sup>2</sup>. Humidity values were kept around 40 % and the temperature was kept bellow 25 °C. Keeping in mind that cellulose is sensitive to humidity, having a strong water absorption, because it has many hydroxyl groups.

Figure 3.8 represents the working mechanism of the EHDs when they suffer the impact from the head of the home-made bending machine. Schematic representation in Figure A.4.

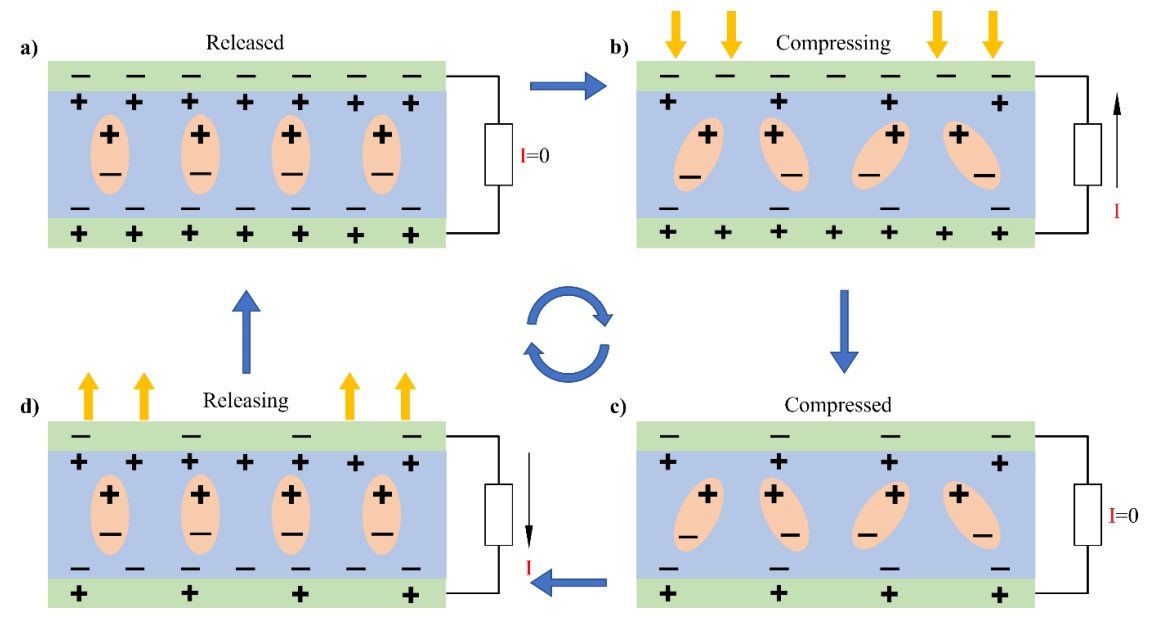


Figure 3.8 - A schematic representation of a regular EHDs' working mechanism. In **a**) before impact (normal state), in **b**) while being compressed, in **c**) totally compressed and in **d**) while being released. Based on [11].

When an external force is applied, compression and recovery will make a change in the dipole moment and change the charge density at the two poles, and electrons are then

transferred through the external circuit to reach charge balance, which results in a piezoelectric current output that can be used to harvest electricity from external forces [11].

Starting off in Figure 3.8 a) in its normal state, released, the EHDs has no induced charge. In Figure 3.8 b), during the compressing phase, from the home-made bending machine, the EHD starts to induce charge in the circuit. When the EHD is fully compressed, in Figure 3.8 c), there is no induced charge in the circuit, because in this phase the EHD is being compressed in a constant way, so there is no transference of electrons. Lastly in Figure 3.8 d) is when the head of the home-made bending machine is retrieving, occurring a decompression which induces again a charge in the circuit on the opposite direction to the previous one in Figure 3.8 b).

Several EHDs were created in two unique structures as shown in **a**) and **b**) in Figure 3.9, illustrating the schematic representation, not to scale, of the two distinctive structures of the EHD produced during this work. The major difference was the type of the electrode used on both sides of the EHD. In Figure 3.9 **a**), the conductive electrode was ITO on PET and in Figure 3.9 **b**), the electrode used was Ag printed on paper. Having in mind that on both cases the electrodes cannot have any contact between them, because if so the EHDs are in short circuit, which is an unintended electrical connection that causes the current to flow immediately from the electrode closest to the impact side to the electrode furthest, resulting in two identical signals from both electrodes, meaning the difference between them is zero and a value for the peak-to-peak voltage is absent.

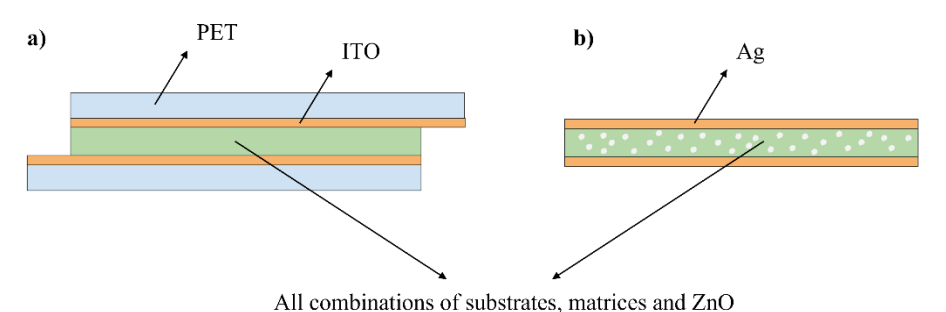


Figure 3.9 - Schematic structures of the two types of substrates of the EHD produced. In **a)** the EHDs build with PET/ITO and in **b)** the EHDs build with Ag electrodes printed on each side of the substrate. Image not to scale.

Represented in green, in the middle of the electrodes, it can be either the control samples (the substrates Navigator or Whatman), one of the three matrices used (PDMS, CMC and EC), or even one of the matrices embedded in one substrate. The white dots represent the ZnO rods mixed with one of the matrices in the situations where it was added, and they, could be used in both structures.

Due to its assembly, the EHDs produced with the structure with PET/ITO electrodes has two or three spaces, depending on the adhesion of the substrate or matrix to the electrodes,

while the structure with Ag electrodes has just one space, between the impact from the home-made bending machine and the force sensor, which is fixed.

The data that the oscilloscope provides comes from two channels, which are two distinct signals coming from two different electrodes on each side of the EHD, and each one of them has its voltage output. There is an option on the oscilloscope, called Math, which is set by hand to simply do the subtraction between both signals, in order to obtain the required curve, the output voltage of the EHD.

Figure 3.10 shows a representative curve of the output voltage of the impact from the bending machine on the EHD. In this case the EHD in question is PET/ITO Whatman CMC ZnO. Two close-ups from the impact area of the EHD are represented, in Figure 3.10 a) the stationary state, where the output voltage is null, as no mechanical force is being applied on the EHD, and in Figure 3.10 b) the compressing and releasing state.

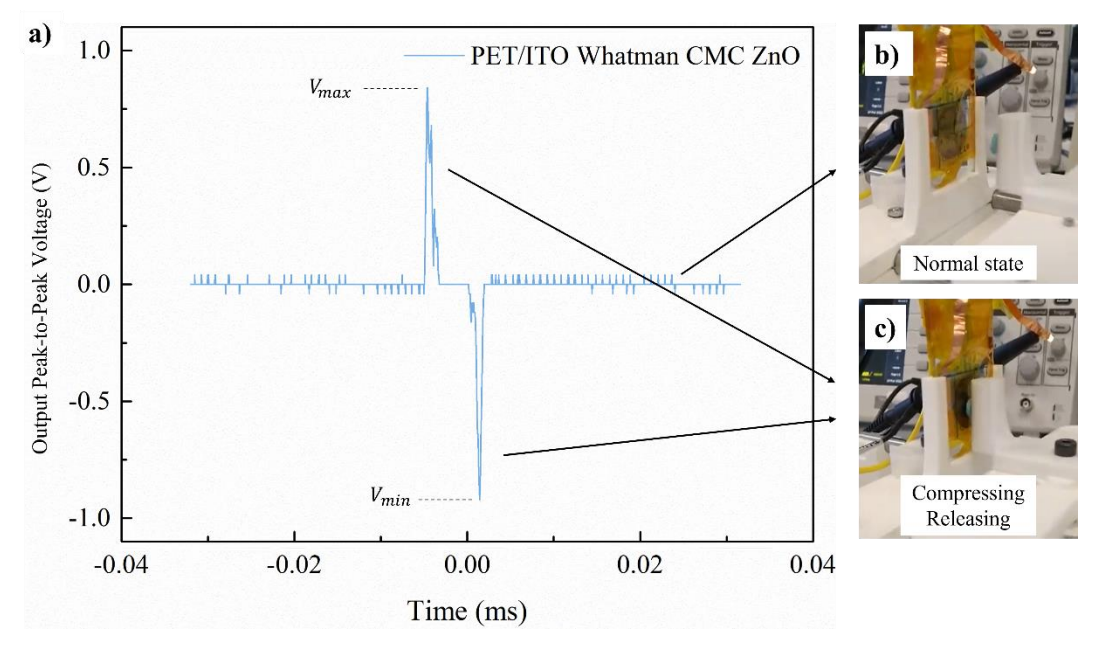


Figure 3.10 - Example of the output voltage coming from one single impact on the EHD. In **a)** A representative output peak-to-peak voltage from the EHDs. With close-ups photographs of the impact area, in **b)** in the normal state and in **c)** the compressing and releasing.

Normally in each curve there are two peaks, that have opposite signs and ideally are equal in module, because the same amount of force in module should be applied during the compressing phase and during the releasing phase. Conventionally the first peak is positive and the second one is negative, as seen in Figure 3.10.

Each type of EHD had two to seven replicas, depending on the abundance of the materials required and from the needed data, and from every single EHD produced, five curves of the output voltage were obtained to be analysed and averaged.

The peak-to-peak output voltage was the more important value to take from the electrical characterization. The peak-to-peak of every EHD was calculated by subtracting the minimum peak value from the maximum peak value.

In some cases, the output voltage from the EHD was null, and this can be justified due to the fact that the EHD was in short circuit, due to some misstep on the production process, some malfunction on a specific layer or even simply the EHD did not present any electrical response.

## 3.3.1 Type of EHDs produced

#### 3.3.1.1 Control EHDs

For comparison purposes, the initial tests were made with control EHDs, where only the substrates alone were studied, Navigator and Whatman, and also the matrices, PDMS, CMC and EC, were analysed with nothing else added. The substrates Navigator and Whatman were assembled in between PET/ITO following the structure in Figure 3.9 a), and with Ag electrodes on each side like in Figure 3.9 b). Two replicas were made of each one. The second type of control EHDs were the ones with the matrices between the PET/ITO electrodes, following the same structure like in Figure 3.9 a).

#### 3.3.1.2 EHDs produced with ZnO

Figure 3.11 shows six photographs of the intermediate stage of the majority of the EHDs produced with ZnO rods. With these embedded substrates ten different types of EHDs were made, seen on Table A.1, on the ZnO classes. Vertically separating the matrices, on the left CMC and on the right EC, and horizontally listing the substrates, from top to bottom, Whatman, Navigator and PET/ITO. Once again, the matrices CMC and EC were better embedded in the substrate Whatman against the substrate Navigator, due to the lower porosity of the second one, leaving a proper layer, well seen in Figure 3.11 c) and d), resulting in a heterogenous substrate. When contrasting both celluloses applied on paper, it is noticeable that after the matrix CMC got embedded, both substrates, Whatman and Navigator, suffered more wrinkle when compared to the matrix EC applied on the same papers. The photographs seen in Figure 3.11 c) and d), were taken at an angle so that the wrinkle effect could be more clearly seen, and the remaining ones were taken from a top viewpoint. To obtain a matrix with evenly dispersed ZnO rods, the mix was magnetically stirred for ten minutes for both cases before drying. When mixed in the CMC matrix, the ZnO rods were better dispersed, getting indeed more scattered and also less aggregated when compared with the same ZnO rods in the same ratio in the EC matrix. This is quite evident in Figure 3.11 b), d) and f), leaving the CMC mixture to be a more homogenous mixture. Only in Figure 3.11 e), is it possible to notice some small

ZnO rods aggregations, because the mix was deposited on PET/ITO, which is super smooth compared to the paper's substrates. Another procedure to mix these ZnO rods on both celluloses needs to be investigated.

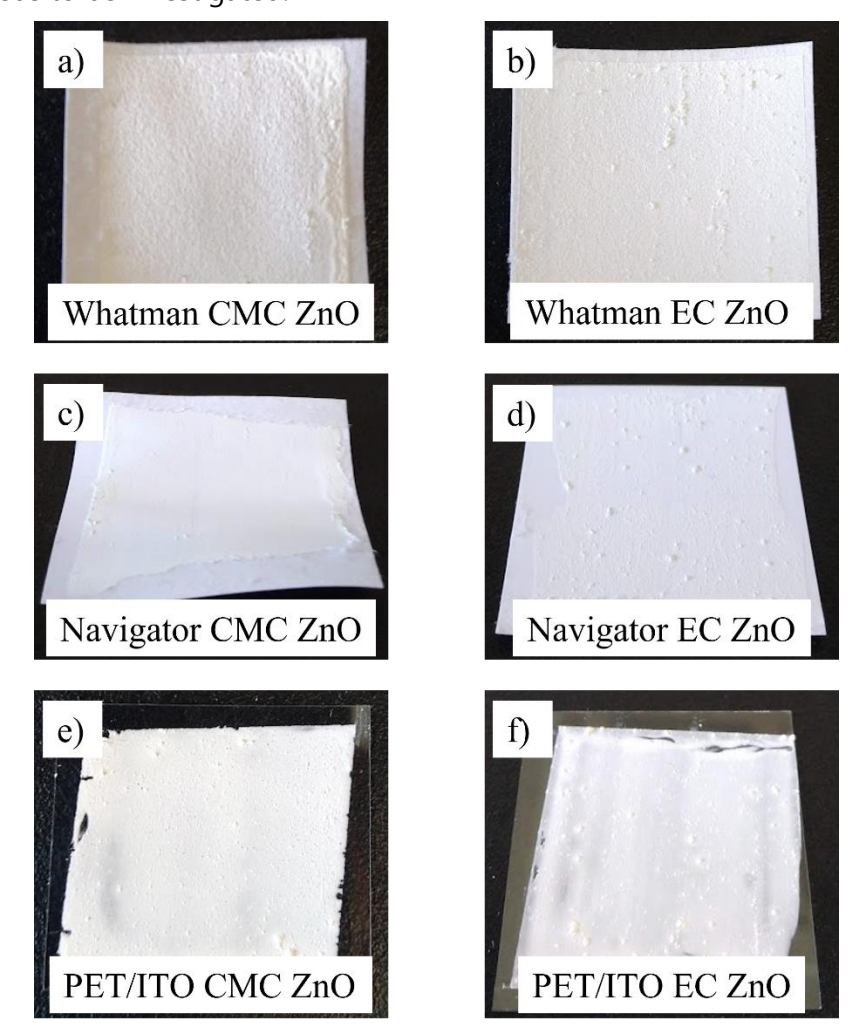


Figure 3.11 - Six photographs of the EHDs after the deposition and drying phase, prior to assembly. On the left side there is the matrix CMC mixed with ZnO and on the right the matrix EC mixed with ZnO, and in a) and b) both were applied in the substrate Whatman, in c) and d), applied in the substrate Navigator and e) and f) the substrate PET/ITO.

At the time of assembly, the embedded substrates with the mixture of celluloses and ZnO rods shown in Figure 3.11 a), b), c) and d) were sandwiched between two PET/ITOs to produce the EHD, being build up in a structure like the one shown in Figure 3.9, leaving unavoidable gaps between layers. Analogous to these ones, the same happened to the e) and f) in Figure 3.11, but in these ones the substrate was one PET/ITO, resulting in a superior adherence to at least this first electrode, when compared with the previous four mentioned, and having the second electrode just added on top, attached with Kapton duct tape. Other four similar embedded substrates as in Figure 3.11 a), b), c) and d), made in the same conditions, had Ag electrodes deposited through the screen-printing method.

#### 3.3.2 Results

### 3.3.2.1 EHDs produced with PET/ITO electrodes without ZnO

Figure 3.12 presents the output peak-to-peak voltage in V from the various combinations of the EHDs produced, following the structure in Figure 3.9 a), consisting firstly of the two substrates and the three matrices solely, and also the combinations of the matrices embedded in the substrates, always between PET/ITO.

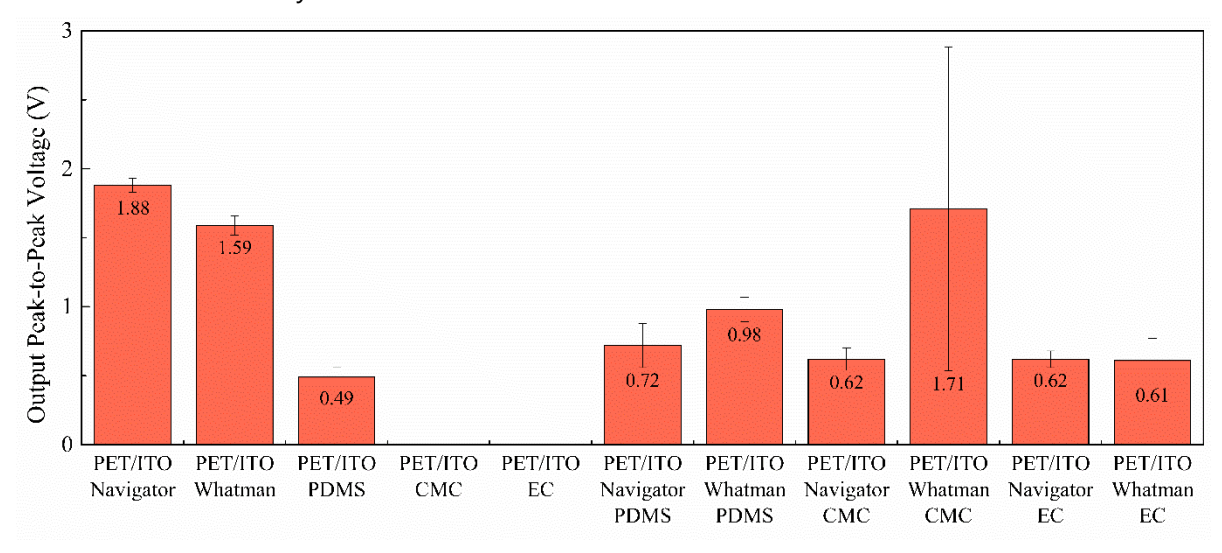


Figure 3.12 - Output peak-to-peak voltage of the EHDs produced with the substrate PET/ITO, starting from the control ones, the two papers and the three matrices solely, and presenting all combinations among them, from left to right.

Firstly, starting with the control EHDs on the left side of the column chart, where the only substrates between the PET/ITO electrodes were papers, the substrate Navigator shows a slightly better average peak-to-peak voltage when compared to the substrate Whatman between PET/ITO electrodes, being the best obtained output voltage of this category. Their average peak-to-peak voltage is (1.88  $\pm$  0.05) V with 3 % error and (1.59  $\pm$  0.07) V with 4 % error, respectively, having a low error associated. Not forgetting the way these EHDs were assembled, with the paper just compacted between the electrodes and not bonded in any manner to either electrode, the peak-to-peak voltage results solely from the triboelectric effect since paper on its own is not a piezoelectric material. Still in the topic of the control EHDs, and regarding the ones with PDMS between PET/ITO electrodes, here the PDMS was applied by an automatic film applicator, unlike a previous work where the PDMS was deposited by spincoating [8]. The results obtained are the following: an average peak-to-peak voltage of (0.49 ± 0.07) V with 12 % associated error, demonstrating a slightly better result compared to that mentioned work. The EHDs produced with either cellulose, CMC or EC, between the electrodes do not show any peak-to-peak response, most probably because both electrodes are in short-circuit, due to the thickness of the cellulose layer being insufficient for these electrodes not to touch. Both EHDs with PDMS embedded in the substrates, Navigator or Whatman, show slightly better results when compared to PDMS alone, and comparing both substrates, Whatman has a superior output voltage, almost reaching 1 V of peak-to-peak voltage. Both EHDs have a triboelectric effect contributing to the transference of electrons, being the embedded paper responsible for it. At last, on this Figure 3.12, the combinations between the embedded matrices on the substrates are shown, where the best result obtained is a peak-to-peak voltage of  $(1.71 \pm 1.17)$  V, from the EHD where the matrix CMC was embedded in the Whatman substrate, also presenting the highest associated error, with 53 %. The others three EHDs show values that are very similar between them and low values for the error.

Looking at all the EHD here analysed it is notable that the control EHD build only with paper showed better results that the majority of the EHDs produced with substrates with embedded matrices. The substrates alone have a rougher surface because of their own fibers, leading to a higher peak-to-peak voltage output. Due to the type of the contact being made with the PET/ITO electrodes, there was a higher triboelectric contribution.

#### 3.3.2.2 EHDs produced with PET/ITO electrodes with ZnO

Figure 3.13 shows the output peak-to-peak voltage in V from the several combinations of the EHDs produced with PET/ITO electrodes and with ZnO rods, following the structure presented in Figure 3.9 a), starting with the mixture of ZnO rods with the three matrices, PDMS, CMC and EC, and two of these mixtures embedded in the substrates, from left to right, all of them between PET/ITO electrodes.

Starting with the EHDs produced with the matrices, PDMS, CMC and EC, with ZnO rods deposited between the electrodes, when first looking at the ones with PDMS there is an increase in the average output peak-to-peak voltage of 74 % when compared to the EHD in the same condition without ZnO rods, again with a low error associated. A value for the average peak-to-peak voltage is obtained for the cellulose-based EHDs, that previously showed no results whatsoever, when mixed with 25 % in weight of ZnO rods.

This value is quite weak for the CMC mixed with ZnO and comparatively very high for the EC mixed with the rods reaching ( $2.0 \pm 1.3$ ) V, although having an error of 46 %. In the following EHDs the impact from the head of the home-made bending machine was done from the side of deposition of the matrix mixed with ZnO rods embedded in substrate.

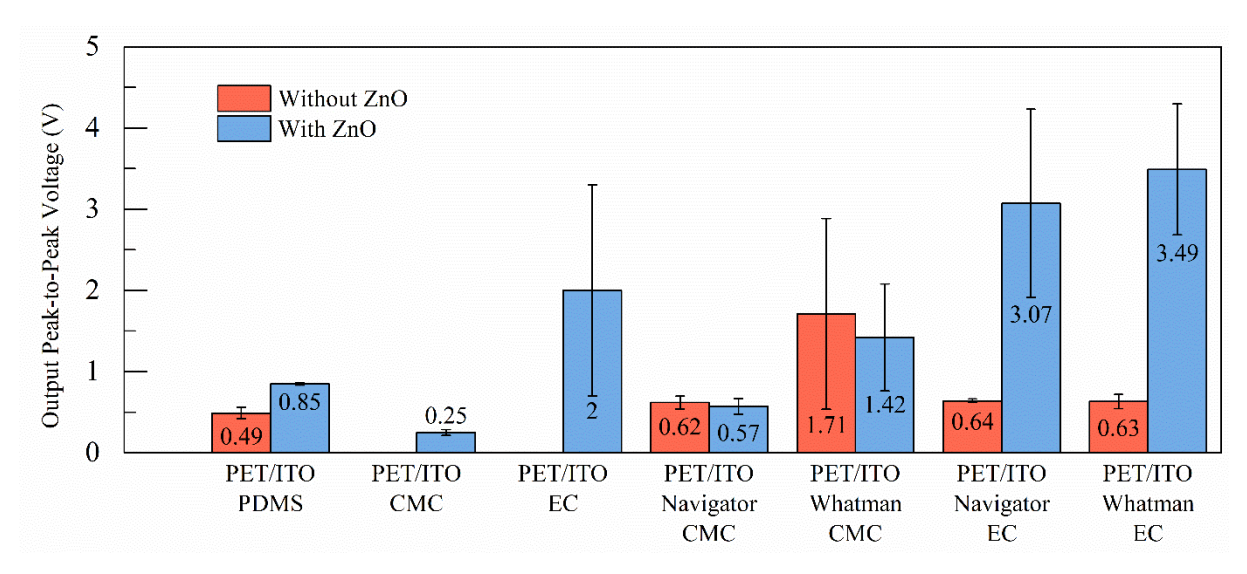


Figure 3.13 - Output peak-to-peak voltage of the EHDs produced with the substrate PET/ITO and with ZnO rods mixed in the matrices, starting from just the matrices and presenting all combinations between the substrates and these matrices with or without ZnO rods, from left to right.

Moving on to the EHDs produced with CMC embedded on both substrates, Navigator and Whatman, practically no difference is seen on the peak-to-peak voltage, when the ZnO rods were added to the matrix. Comparing the EHD produced with EC mixed without ZnO rods and the ones with ZnO rods embedded in the substrates, there is an enormous increase in the peak-to-peak output voltage on both papers, 380 % and 454 %, respectively when Navigator or Whatman was used. This improvement of the peak-to-peak voltage obtained is due to the piezoelectric properties of the ZnO rods mixed with EC. Being Whatman the best result obtained during this dissertation with a peak-to-peak average value of  $(3.5 \pm 0.8)$  V with a 19 % associated error. Showing that the best result came from the EHD produced with ZnO rods mixed with EC embedded in the substrate Whatman between PET/ITO electrodes.

While looking at the error bar in each EHD from Figure 3.13, it is noticeable that the relatively high error is associated with the highest values obtained, showing that the type of electrode chosen is very important to decide if the method is precise or not.

In Figure 3.14, one of the best results obtain during this work is shown, being from the substrate Whatman embedded with the matrix EC mixed with ZnO rods between PET/ITO electrodes, reaching a peak-to-peak voltage of 7.4 V.

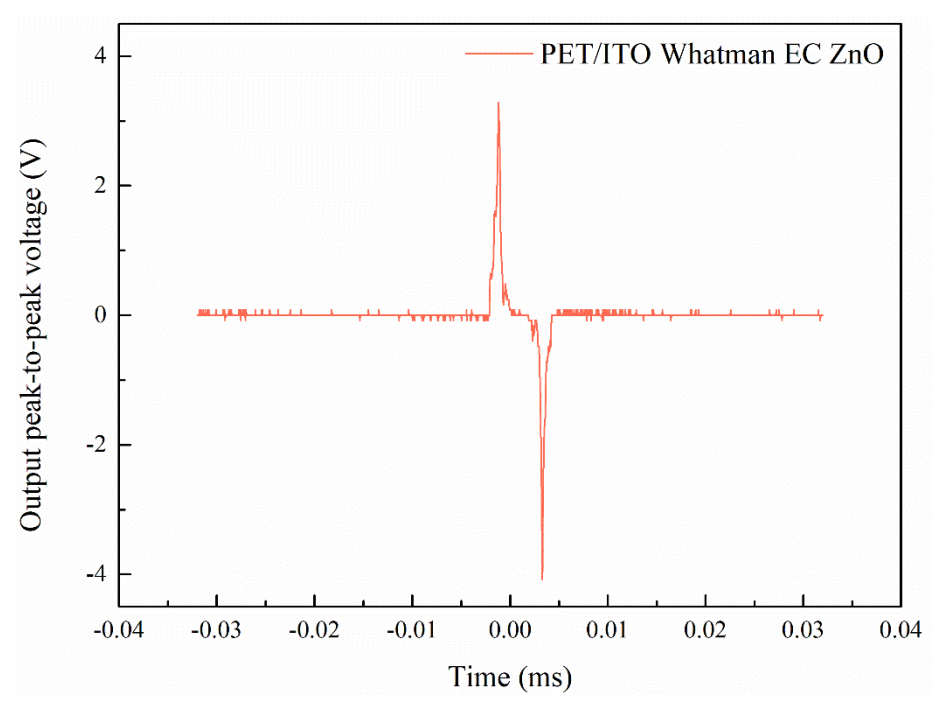


Figure 3.14 - One of the greatest peak-to-peak voltage obtain during this dissertation, being from the substrate Whatman embedded with the matrix EC mixed with ZnO rods, which reached the best output voltage.

#### 3.3.2.3 EHDs produced with Ag electrodes with and without ZnO

Figure 3.15 displays the output voltage in V from the several combinations of the EHDs produced with Ag electrodes, with and without ZnO rods, this time following the structure showed in Figure 3.9 b). From left to right are shown the following types of EHDs: the control, the matrices embedded on the substrates, and the same matrices with ZnO rods mixed in them embedded again on the substrates.

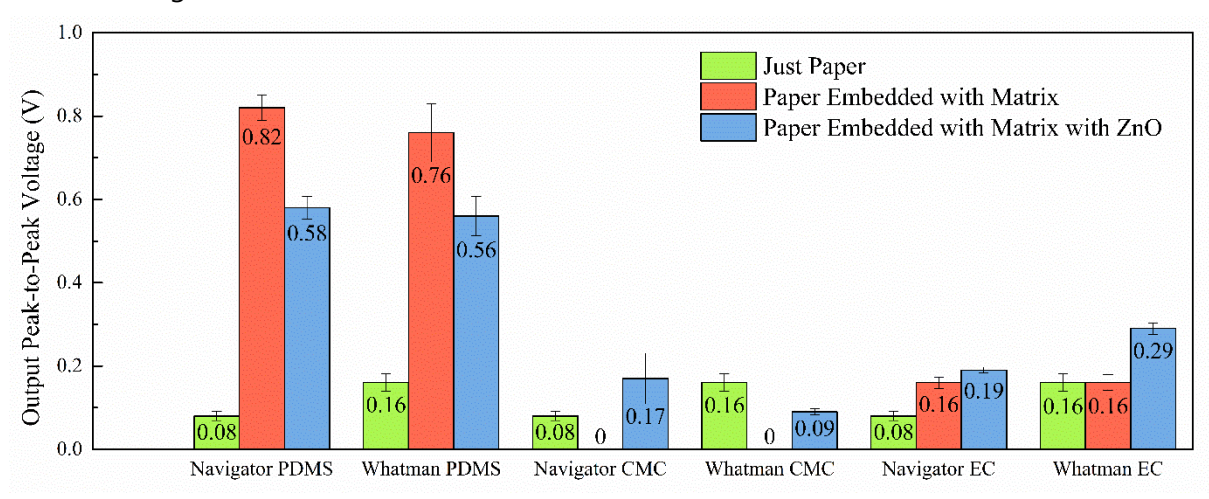


Figure 3.15 - Output peak-to-peak voltage of the EHDs produced with Ag electrodes. In green the EHDs with solely the substrates, Navigator and Whatman, are presented, in red the EHDs with the substrates embedded with a matrix are presented and lastly in blue the paper embedded with the matrix with ZnO rods are presented.

Starting from left to right, firstly there are the control EHDs, where only the papers alone with the printed Ag electrode were analysed, obtaining low results for the output peak-to-peak

voltage, being the substrate Whatman slightly higher when comparing to Navigator, only reaching (0.16  $\pm$  0.02) V with a 14 % associated error. As paper alone is not a piezoelectric material, this value must come directly from the triboelectric contribution, due to the gap between the EHD and the force sensor. Proceeding to the EHDs with deposited PDMS on one side, both substrates had similar results on their peak-to-peak performance, with the substrate Navigator being the better one this time, with (0.82  $\pm$  0.03) V of output voltage and a low associated error of 3 %. Moving to the EHDs produced with each cellulose, CMC or EC, the CMC ones showed no output voltage while receiving mechanical load. This can be explained by the fact that the electrodes might at some point, throughout either side of the EHD, be in contact. With the decrease in the thickness of the EHDs from the embedded celluloses, already discussed in 3.2.2, the Ag particles can enter the remaining pores with moderate ease, short circuiting the EHD, example of this seen in Figure 3.16.

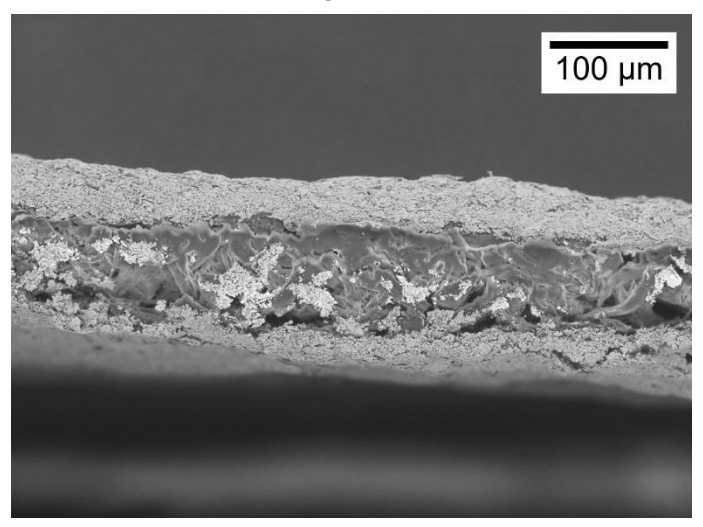


Figure 3.16 - A cross section SEM image of the EHD with the matrix CMC embedded in the substrate Whatman with Ag electrodes applied by screen printing.

The outcome of EHDs using EC as the embedded matrix was the same for both substrates, which was an extremely low output voltage. When the ZnO rods were added to the matrix PDMS and embedded in the substrates, there was a decrease of 30 % and 27 % in the average peak-to-peak value on the substrate Navigator and Whatman, respectively. Looking at the EHDs build with either cellulose as a matrix mixed with ZnO rods, they showed low peak-to-peak values. Firstly CMC, where previously no output voltage was seen, and with ZnO rods incorporated a small peak-to-peak was obtained, being Navigator the better substrate with  $(0.17 \pm 0.06)$  V peak voltage with a 23 % of associated error. While with EC, the best result was from the substrate Whatman, with also a small result,  $(0.29 \pm 0.01)$  V with a low error of 5 %. SEM cross section images of the six EHDs with ZnO mixed in the embedded matrices can be seen in Figure A.6.

All of the EHDs produced with Ag electrodes present a relatively low error associated with the output voltage measure, this is due to the fact that EHDs build like this only have one gap when they are under electric characterization, between the EHD itself and the force sensor, decreasing the triboelectric effect and per consequence decreasing the error involving the manual attachment of the EHD to the force sensor, seen in Figure A.3.

At the time of deposition of the Ag electrode on the EHDs its adhesion with the substrate, whether if it had a matrix embedded or not, is of highly importance. Looking at the control samples, the Ag adhered quite well when compared with the same substrates, Navigator and Whatman, with PDMS deposited on its surface. On these last EHDs the adhesion was mediocre and on the substrate Navigator was worse comparing to the substrate Whatman, requiring the application of a UV treatment in order to increase the Ag's adhesion to the EHDs. The following equipment, Novascan PSD-UV, PSDP-UV and PSDP-UVT, UV/Ozone Systems, was employed for said UV treatment. The UV method involved a simple illumination of ultraviolet for 5 min at room temperature on the substrate Navigator with PDMS deposited. This procedure changes the hydrophobicity of the EHD's surface. When applied on EHDs with the embedded matrices, CMC and EC, the adhesion of the Ag electrodes was great.

In the case of the Ag electrodes that have a discontinuity of the material itself, a crack for example, an electrical discontinuity will take place, possibly resulting in a null output voltage from the EHD.

When looking at all column charts presented and comparing the respective standard deviations from every EHDs, it was concluded that from the 28 different types of devices, that showed results, 13 of them had an associated error under 10 %.

Putting side by side the average error value of all EHDs, a significant difference was seen. Contraposing the ones with PET/ITO as the electrode and the ones with Ag electrodes, respectively, having an average error of 24 % and 9 %. Potentially since the EHDs produced with PET/ITO electrodes have more layers in them, which translates in gaps between them, resulting in a higher corresponding triboelectric contribution and inconstancy, due to the way that the EHD is attached to the support where it is tested, seen in Figure A.3.

4

# **CONCLUSIONS AND FUTURE PERSPECTIVES**

This dissertation provides a new approach for the concept of sustainable energy harvesting system devices, where flexible, low-cost, and environmentally friendly EHDs were produced, with an accessible, easy, low-cost, and fast method of production. The devices made included mainly paper-based features which supports all the sustainable goals targeted. These devices are able to convert mechanical energy into electrical energy. In total, 116 EHDs were made, making up 32 different types of EHDs. Two types of electrodes were investigated, PET/ITO and Ag electrodes, as well as two substrates, Navigator and Whatman, both commercial papers. Furthermore, three matrices were studied, PDMS, CMC and EC, and additionally, these matrices were mixed with pure ZnO rods, as seen during this work. The method used herein for ZnO production is low-cost, sustainable, and reproductible, with the measurements across different synthesis showing a normal distribution pattern with coinciding averages values for length and diameter,  $(3.97 \pm 1.59) \mu m$  and  $(440 \pm 168) nm$ , respectively. Furthermore, the fabrication method only requires abundant and cheap materials, producing ZnO rods with piezoelectric properties and with a high level of crystallinity, as supported by the XRD results.

Two types of EHDs designs were studied with the main difference being the electrode used, one based on PET/ITO electrodes and one based on Ag electrodes screen-printed directly on the substrate, aiming for a sustainable option, due to the materials involved. However, the performance of the EHDs with Ag electrodes was lower than that of the EHDs with PET/ITO electrodes, despite their higher flexibility. A justification for this low output value can be the fact that the structure itself has less layers of materials, which means less gaps between them, reducing the contribution of the triboelectric effect on the output value of the EHD. The best output results obtained in the category of the Ag electrodes EHDs was from the ones with PDMS, which reached a peak-to-peak voltage of  $(0.82 \pm 0.03)$  V. This can be due to the individual layer that the PDMS itself created upon impregnation in the papers, preventing the migration of silver particles between the printed electrodes. Contrarily, when CMC or EC were impregnated in the papers, silver particles may have migrated from one electrode to the other, contributing to paths for current leakage and, thus, a reduction of the output. The highest peak-to-peak result obtained from all the EHDs produced was from the EHD based on Whatman paper embedded with the matrix EC mixed with ZnO rods between PET/ITO electrodes, reaching an average voltage of 3.5 V.

Both papers herein studied had distinct features, such as porosity and thickness, to investigate the most suitable to maximize the peak-to-peak voltage. Before the electrical characterization,

it was expectable that the best paper would be the less porous one, the Navigator, because this one would have a better surface for the electrodes printing. Nonetheless, this supposition was not confirmed, since the Whatman paper was slightly better in some of the EHDs configurations. This observation may be explained by the higher porosity of Whatman paper, which led to a better impregnation of the composites of matrix and ZnO rods, and consequent accumulation of more ZnO rods throughout the thickness of the EHD. Adding to this, the Whatman paper has a more irregular surface, a factor that contributes to the triboelectric effect.

In this work, three matrices were analysed, the first one being PDMS, a matrix previously used in the composition of EHDs, and two celluloses, EC and CMC. These 3 matrices showed different levels of impregnation. The least impregnated one was PDMS, while the most impregnated one was EC. EHDs with PDMS showed the higher final thickness, followed by the EHDs with CMC, and the lowest thickness was verified with EC. The deposition of the PDMS matrix on the substrate was very heterogenous, comparing to the deposition of both celluloses, which was more homogeneous throughout the thickness of the substrate. In general, the best outputs obtained were from the EHDs with the EC matrix.

Even if the results from the sustainable EHDs produced herein are optimistic, the technology still has room for improvement. Keeping that in mind, significant progress has already been done on this subject during the course of this thesis:

- 1. Characterization of the ZnO rods obtained by hydrothermal synthesis assisted by microwave irradiation;
  - 2. Dimensional and topographical characterization of the embedded substrates;
  - 3. Using papers as the substrate;
  - 4. Incorporating celluloses in energy harvesting devices, as a replacement for PDMS;
  - 5. Mixing ZnO rods with the cellulose.

As **future perspectives** some procedures can be improved, such as the mixing of the ZnO rods with both celluloses, which were only magnetically agitated for ten minutes. Maybe letting this agitation for a longer period, for example 24 h, would improve the dispersing of the ZnO rods.

It is necessary to find better electrodes to enhance the maximum output voltage of the EHDs, with a better transference of electrons, since the Ag electrodes turned out to reach lower voltages when compared to the PET/ITO ones.

Also, for following up works, several parameters can be studied like varying the cellulose concentration in weight. Herein, 3 % in weight of CMC and 5 % in weight of EC were studied, but other concentrations can turn out to be more effective. Also, more than just one layer can be applied, meaning multiple layers of these celluloses can be studied, and additionally, depositing layers on both sides of the EHDs can enhance the maximum output voltage.

The EHDs on this work were unstructured, unlike others already made in the literature. In fact, they were all closer to a flat substrate, except for the ones where the celluloses were added, specially with CMC embedded in the substrates. In this case, the embedded substrates presented a larger wrinkling effect. Perhaps creating a surface with some kind of pattern, wavy for example, for the embedded paper to dry into such a shape, can later help to improve the maximum output voltage, with a hybrid regime of both piezoelectricity and triboelectricity, seen in more detail in A.7.

# **BIBLIOGRAPHY**

- [1] P. Butler, *Smart and interactive packaging developments for enhanced communication at the packaging/user interface*. Woodhead Publishing Limited, 2013. doi: 10.1533/9780857098979.261.
- [2] J. Gao, Z. Pang, Q. Chen, and L. R. Zheng, 'Interactive packaging solutions based on RFID technology and controlled delamination material', *RFID 2010 Int. IEEE Conf. RFID*, no. March 2015, pp. 158–165, 2010, doi: 10.1109/RFID.2010.5467270.
- [3] Z. Fang, Y. Zhao, R. D. Warner, and S. K. Johnson, 'Active and intelligent packaging in meat industry', *Trends Food Sci. Technol.*, vol. 61, no. 2, pp. 60–71, 2017, doi: 10.1016/j.tifs.2017.01.002.
- [4] S. Yildirim *et al.*, 'Active Packaging Applications for Food', *Compr. Rev. Food Sci. Food Saf.*, vol. 17, no. 1, pp. 165–199, Jan. 2018, doi: 10.1111/1541-4337.12322.
- [5] P. Reynolds, 'Electroluminescent packaging', 2013. https://www.packworld.com/home/article/13362773/electroluminescent-packaging (accessed Feb. 15, 2022).
- [6] 'SaralSensor©'. https://www.saralon.com/en/applications/saralsensor/ (accessed Feb. 15, 2022).
- [7] A. Dos Santos *et al.*, 'Optimization of zno nanorods concentration in a micro-structured polymeric composite for nanogenerators', *Chemosensors*, vol. 9, no. 2, pp. 1–13, 2021, doi: 10.3390/chemosensors9020027.
- [8] A. Rovisco *et al.*, 'Piezoelectricity Enhancement of Nanogenerators Based on PDMS and ZnSnO3Nanowires through Microstructuration', *ACS Appl. Mater. Interfaces*, vol. 12, no. 16, pp. 18421–18430, 2020, doi: 10.1021/acsami.9b21636.
- [9] A. Plesa, I. V. Iancu, A. Botezatu, I. Huica, M. Stoian, and G. Anton, 'Porous ZnO Nanostructures Synthesized by Microwave Hydrothermal Method for Energy Harvesting Applications', *Intech*, vol. i, no. tourism, p. 13, 2016.
- [10] B. Saravanakumar, R. Mohan, K. Thiyagarajan, and S. J. Kim, 'Fabrication of a ZnO nanogenerator for eco-friendly biomechanical energy harvesting', *RSC Adv.*, vol. 3, no. 37, pp. 16646–16656, 2013, doi: 10.1039/c3ra40447a.
- [11] Y. Song, Z. Shi, G. H. Hu, C. Xiong, A. Isogai, and Q. Yang, 'Recent advances in cellulose-based piezoelectric and triboelectric nanogenerators for energy harvesting: a review', *J. Mater. Chem. A*, vol. 9, no. 4, pp. 1910–1937, 2021, doi: 10.1039/d0ta08642h.
- [12] S. Chandrasekaran *et al.*, 'Micro-scale to nano-scale generators for energy harvesting: Self powered piezoelectric, triboelectric and hybrid devices', *Phys. Rep.*, vol. 792, pp. 1–33, 2019, doi: 10.1016/j.physrep.2018.11.001.
- [13] Y. Zi *et al.*, 'Triboelectric-pyroelectric-piezoelectric hybrid cell for high-efficiency energy-harvesting and self-powered sensing', *Adv. Mater.*, vol. 27, no. 14, pp. 2340–2347, Apr. 2015, doi: 10.1002/adma.201500121.
- [14] 'Electricity explained', *How electricity is generated*, 2021. https://www.eia.gov/energyexplained/electricity/how-electricity-is-generated.php (accessed Feb. 14, 2022).
- [15] A. S, 'solar energy', *The Editors of Encyclopaedia Britannica*. https://www.britannica.com/science/solar-energy/Electricity-generation (accessed Feb. 16, 2022).
- [16] E. Boechler, J. Hanania, Jordan Jenden, K. Stenhouse, L. V. Suarez, and J. Donev, 'Coal

- fired power plant'. https://energyeducation.ca/encyclopedia/Coal\_fired\_power\_plant (accessed Feb. 16, 2022).
- [17] P. Glynne-Jones, S. P. Beeby, and N. M. White, 'Towards a piezoelectric vibration-powered microgenerator', *IEE Proc. Sci. Meas. Technol.*, vol. 148, no. 2, pp. 68–72, 2001, doi: 10.1049/jp-smt:20010323.
- [18] D. L. Churchill, M. J. Hamel, C. P. Townsend, and S. W. Arms, 'Strain energy harvesting for wireless sensor networks', *Smart Struct. Mater. 2003 Smart Electron. MEMS, BioMEMS, Nanotechnol.*, vol. 5055, p. 319, 2003, doi: 10.1117/12.483591.
- [19] Z. L. Wang and J. Song, 'Piezoelectric nanogenerators based on zinc oxide nanowire arrays', *Science (80-. ).*, vol. 312, no. 5771, pp. 242–246, 2006, doi: 10.1126/science.1124005.
- [20] F. R. Fan, Z. Q. Tian, and Z. Lin Wang, 'Flexible triboelectric generator', *Nano Energy*, vol. 1, no. 2, pp. 328–334, 2012, doi: 10.1016/j.nanoen.2012.01.004.
- [21] H. Zhang, Y. Yang, T. C. Hou, Y. Su, C. Hu, and Z. L. Wang, 'Triboelectric nanogenerator built inside clothes for self-powered glucose biosensors', *Nano Energy*, vol. 2, no. 5, pp. 1019–1024, 2013, doi: 10.1016/j.nanoen.2013.03.024.
- [22] Z. L. Wang, 'Triboelectric nanogenerators as new energy technology and self-powered sensors Principles, problems and perspectives', *Faraday Discuss.*, vol. 176, no. 11, pp. 447–458, 2014, doi: 10.1039/C4FD00159A.
- [23] S. Lee *et al.*, 'Super-flexible nanogenerator for energy harvesting from gentle wind and as an active deformation sensor', *Adv. Funct. Mater.*, vol. 23, no. 19, pp. 2445–2449, 2013, doi: 10.1002/adfm.201202867.
- [24] L. Lin *et al.*, 'Transparent flexible nanogenerator as self-powered sensor for transportation monitoring', *Nano Energy*, vol. 2, no. 1, pp. 75–81, 2013, doi: 10.1016/j.nanoen.2012.07.019.
- [25] S. H. Shin, M. H. Lee, J. Y. Jung, J. H. Seol, and J. Nah, 'Piezoelectric performance enhancement of ZnO flexible nanogenerator by a CuO-ZnO p-n junction formation', *J. Mater. Chem. C*, vol. 1, no. 48, pp. 8103–8107, 2013, doi: 10.1039/c3tc31664e.
- [26] P. X. Gao, J. Song, J. Liu, and Z. L. Wang, 'Nanowire piezoelectric nanogenerators on plastic substrates as flexible power sources for nanodevices', *Adv. Mater.*, vol. 19, no. 1, pp. 67–72, 2007, doi: 10.1002/adma.200601162.
- [27] C. Wu, A. C. Wang, W. Ding, H. Guo, and Z. L. Wang, 'Triboelectric Nanogenerator: A Foundation of the Energy for the New Era', *Adv. Energy Mater.*, vol. 9, no. 1, p. 1802906, Jan. 2019, doi: 10.1002/aenm.201802906.
- [28] G. Gautschi, *Piezoelectric Sensorics*. Berlin, Heidelberg: Springer Berlin Heidelberg, 2002. doi: 10.1007/978-3-662-04732-3.
- [29] L. Lin *et al.*, 'An elastic-spring-substrated nanogenerator as an active sensor for self-powered balance', *Energy Environ. Sci.*, vol. 6, no. 4, pp. 1164–1169, 2013, doi: 10.1039/c3ee00107e.
- [30] X. Jiang, W. Huang, and S. Zhang, 'Flexoelectric nano-generator: Materials, structures and devices', *Nano Energy*, vol. 2, no. 6, pp. 1079–1092, 2013, doi: 10.1016/j.nanoen.2013.09.001.
- [31] J. H. J. H. Lee *et al.*, 'Micropatterned P(VDF-TrFE) film-based piezoelectric nanogenerators for highly sensitive self-powered pressure sensors', *Adv. Funct. Mater.*, vol. 25, no. 21, pp. 3203–3209, 2015, doi: 10.1002/adfm.201500856.
- [32] X. Chen *et al.*, 'A wave-shaped hybrid piezoelectric and triboelectric nanogenerator based on P(VDF-TrFE) nanofibers', *Nanoscale*, vol. 9, no. 3, pp. 1263–1270, 2017, doi:

- 10.1039/c6nr07781a.
- [33] G. Zhu *et al.*, 'Linear-grating triboelectric generator based on sliding electrification', *Nano Lett.*, vol. 13, no. 5, pp. 2282–2289, 2013, doi: 10.1021/nl4008985.
- [34] Y. Yang *et al.*, 'Single-electrode-based sliding triboelectric nanogenerator for self-powered displacement vector sensor system', *ACS Nano*, vol. 7, no. 8, pp. 7342–7351, 2013, doi: 10.1021/nn403021m.
- [35] S. Wang, L. Lin, and Z. L. Wang, 'Nanoscale triboelectric-effect-enabled energy conversion for sustainably powering portable electronics', *Nano Lett.*, vol. 12, no. 12, pp. 6339–6346, 2012, doi: 10.1021/nl303573d.
- [36] S. Wang, Y. Xie, S. Niu, L. Lin, and Z. L. Wang, 'Freestanding triboelectric-layer-based nanogenerators for harvesting energy from a moving object or human motion in contact and non-contact modes', *Adv. Mater.*, vol. 26, no. 18, pp. 2818–2824, 2014, doi: 10.1002/adma.201305303.
- [37] Z. L. Wang, J. Chen, and L. Lin, 'Progress in triboelectric nanogenerators as a new energy technology and self-powered sensors', *Energy Environ. Sci.*, vol. 8, no. 8, pp. 2250–2282, 2015, doi: 10.1039/c5ee01532d.
- [38] S. Nandy *et al.*, 'Cellulose: A Contribution for the Zero e-Waste Challenge', *Adv. Mater. Technol.*, vol. 6, no. 7, pp. 1–59, 2021, doi: 10.1002/admt.202000994.
- [39] H. Y. Choi and Y. G. Jeong, 'Microstructures and piezoelectric performance of ecofriendly composite films based on nanocellulose and barium titanate nanoparticle', *Compos. Part B Eng.*, vol. 168, no. April 2018, pp. 58–65, 2019, doi: 10.1016/j.compositesb.2018.12.072.
- [40] P. Szperlich, M. Nowak, and D. Stro, 'Novel piezoelectric paper based on SbSI nanowires', pp. 7–15, 2018, doi: 10.1007/s10570-017-1597-y.
- [41] W. Kang, Y. Li, Z. Zheng, and R. Zhao, 'Enhanced dielectric and piezoelectric performance of (1-x)Bi0.5(Na0.78K0.22)0.5TiO3-xBaTiO3 ceramics', *Ceram. Int.*, vol. 46, no. 11, pp. 18089–18095, 2020, doi: 10.1016/j.ceramint.2020.04.128.
- [42] X. Zhou *et al.*, 'All 3D-printed stretchable piezoelectric nanogenerator with non-protruding kirigami structure', *Nano Energy*, vol. 72, p. 104676, 2020, doi: 10.1016/j.nanoen.2020.104676.
- [43] G. Zhang *et al.*, 'Flexible three-dimensional interconnected piezoelectric ceramic foam based composites for highly efficient concurrent mechanical and thermal energy harvesting', *Energy Environ. Sci.*, vol. 11, no. 8, pp. 2046–2056, 2018, doi: 10.1039/c8ee00595h.
- [44] C. Wan and C. R. Bowen, 'Multiscale-structuring of polyvinylidene fluoride for energy harvesting: the impact of molecular-, micro- and macro-structure', *J. Mater. Chem. A*, vol. 5, no. 7, pp. 3091–3128, 2017, doi: 10.1039/c6ta09590a.
- [45] X. Liu, J. Ma, X. Wu, L. Lin, and X. Wang, 'Polymeric Nanofibers with Ultrahigh Piezoelectricity via Self-Orientation of Nanocrystals', *ACS Nano*, vol. 11, no. 2, pp. 1901–1910, 2017, doi: 10.1021/acsnano.6b07961.
- [46] D. Cavallini, M. Fortunato, G. De Bellis, and M. S. Sarto, 'PFM Characterization of Piezoelectric PVDF / ZnO- Nanorod thin films', pp. 19–21, 2018.
- [47] Z. Sun, L. Yang, S. Liu, J. Zhao, Z. Hu, and W. Song, 'A green triboelectric nano-generator composite of degradable cellulose, piezoelectric polymers of PVDF/PA6, and nanoparticles of BaTiO3', *Sensors (Switzerland)*, vol. 20, no. 2, 2020, doi: 10.3390/s20020506.
- [48] R. Farhan, M. Rguiti, A. Eddiai, M. Mazroui, M. Meddad, and C. Courtois, 'Evaluation of

- performance of polyamide/lead zirconate titanate composite for energy harvesters and actuators', *J. Compos. Mater.*, vol. 53, no. 3, pp. 345–352, 2019, doi: 10.1177/0021998318783324.
- [49] G. Zhu, R. Yang, S. Wang, and Z. L. Wang, 'Flexible high-output nanogenerator based on lateral ZnO nanowire array', *Nano Lett.*, vol. 10, no. 8, pp. 3151–3155, 2010, doi: 10.1021/nl101973h.
- [50] X. Wang, J. Song, J. Liu, and L. W. Zhong, 'Direct-current nanogenerator driven by ultrasonic waves', *Science (80-. ).*, vol. 316, no. 5821, pp. 102–105, 2007, doi: 10.1126/science.1139366.
- [51] E. Commission *et al.*, *Critical raw materials for strategic technologies and sectors in the EU: a foresight study.* Publications Office, 2020. doi: doi/10.2873/58081.
- [52] C. Zhang and Z. L. Wang, *Triboelectric Nanogenerators*. 2018. doi: 10.1007/978-981-10-5945-2\_38.
- [53] J. Park, Y. Lee, M. Ha, S. Cho, and H. Ko, 'Micro/nanostructured surfaces for self-powered and multifunctional electronic skins', *J. Mater. Chem. B*, vol. 4, no. 18, pp. 2999–3018, 2016, doi: 10.1039/c5tb02483h.
- [54] D. Vera, T. He, C. Lee, and M. R. Yuce, 'Nano Energy Self-powered eye motion sensor based on triboelectric interaction and near-field electrostatic induction for wearable assistive technologies', *Nano Energy*, vol. 72, no. January, p. 104675, 2020, doi: 10.1016/j.nanoen.2020.104675.
- [55] F. Fan, L. Lin, G. Zhu, W. Wu, R. Zhang, and Z. L. Wang, 'Transparent Triboelectric Nanogenerators and Self-Powered Pressure Sensors Based on Micropatterned Plastic Films', 2012.
- [56] X. Kang, C. Pan, Y. Chen, and X. Pu, 'Boosting performances of triboelectric nanogenerators by optimizing dielectric properties and thickness of electri fi cation layer +', pp. 17752–17759, 2020, doi: 10.1039/d0ra02181d.
- [57] T. He, X. Guo, and C. Lee, 'iScience II Flourishing energy harvesters for future body sensor network: from single to multiple energy sources', *ISCIENCE*, vol. 24, no. 1, p. 101934, 2021, doi: 10.1016/j.isci.2020.101934.
- [58] X. Shi, S. Zhang, and S. Gong, 'A self-powered and arch-structured triboelectric nanogenerator for portable electronics and human-machine communication', vol. 6, 2020, doi: 10.1039/d0ta02178d.
- [59] S. Yan, K. Dong, J. Lu, W. Song, and R. Xiao, 'Amphiphobic triboelectric nanogenerators based on silica enhanced thermoplastic polymeric nanofiber membranes', *Nanoscale*, vol. 12, no. 7, pp. 4527–4536, 2020, doi: 10.1039/c9nr09925e.
- [60] J. W. Lee *et al.*, 'High-Output Triboelectric Nanogenerator Based on Dual Inductive and Resonance Effects-Controlled Highly Transparent Polyimide for Self-Powered Sensor Network Systems', *Adv. Energy Mater.*, vol. 9, no. 36, pp. 1–11, 2019, doi: 10.1002/aenm.201901987.
- [61] Z. H. Lin, G. Cheng, S. Lee, K. C. Pradel, and Z. L. Wang, 'Harvesting water drop energy by a sequential contact-electrification and electrostatic-induction process', *Adv. Mater.*, vol. 26, no. 27, pp. 4690–4696, 2014, doi: 10.1002/adma.201400373.
- [62] T. Jesionowski, 'Zinc Oxide From Synthesis to Application: A Review', pp. 2833–2881, 2014, doi: 10.3390/ma7042833.
- [63] K. Mohan, B. Kumar, E. Appala, M. Sinha, K. Siva, and P. Sreedhara, 'Spectrochimica Acta Part A: Molecular and Biomolecular Spectroscopy Synthesis and characterisation of flower shaped Zinc Oxide nanostructures and its antimicrobial activity', *Spectrochim.*

- *ACTA PART A Mol. Biomol. Spectrosc.*, vol. 104, pp. 171–174, 2013, doi: 10.1016/j.saa.2012.11.025.
- [64] E. Circular, B. Casos, and D. E. E. Bcsd, 'CASO DE ESTUDO ECONOMIA CIRCULAR Valorização de Lamas de Carbonato no Processo de Produção de Papel', 2020.
- [65] EMERGE, 'Home-made screen-printing system', *Home-made screen-printing system*, 2022. https://emerge-infrastructure.eu/service/home-made-screen-printing-system/ (accessed Aug. 24, 2022).
- [66] P. J. Wojcik, 'Printable organic and inorganic materials for flexible electrochemical devices'.



# A.1 Screen printing illustrative scheme

The equipment employed is custom-made and used for the deposition of films on flexible substrates (such as paper, cloth, cork, glass, and plastic). Commercial pastes can be used (such as carbon, silver, dielectric, thermochromic, etc.) and custom formulations are available in a made-to-order, user-friendly, and portable screen-printing machine (e.g. electrolytes, metal oxide nanostructures, conductive polymers). [65] Some specifications of the equipment: controlled manually, squeegee head, screen adapters, max print area of: 10 cm x 29.7 cm, max substrate size of: A4 size, max screen size of: 46 cm x 66 cm, minimum feature size of:  $\approx 150 \text{ }\mu\text{m}$  (depending on the ink), alignment accuracy of:  $\pm 150 \text{ }\mu\text{m}$ , ink viscosity from: 300 cp to 50000 cp [65].

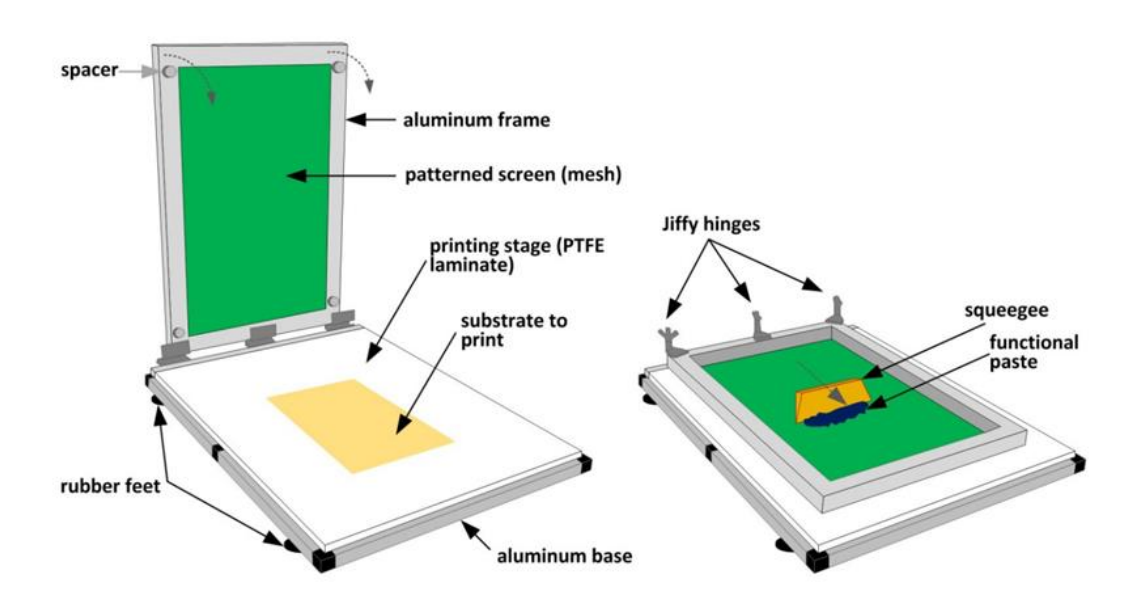


Figure A.1 - Illustrative screen printing scheme of a homemade system [66].

# A.2 Home-made bending machine

A home-made bending machine programmable with several impact heads and a free moving support for the EHD to be tested is shown below.

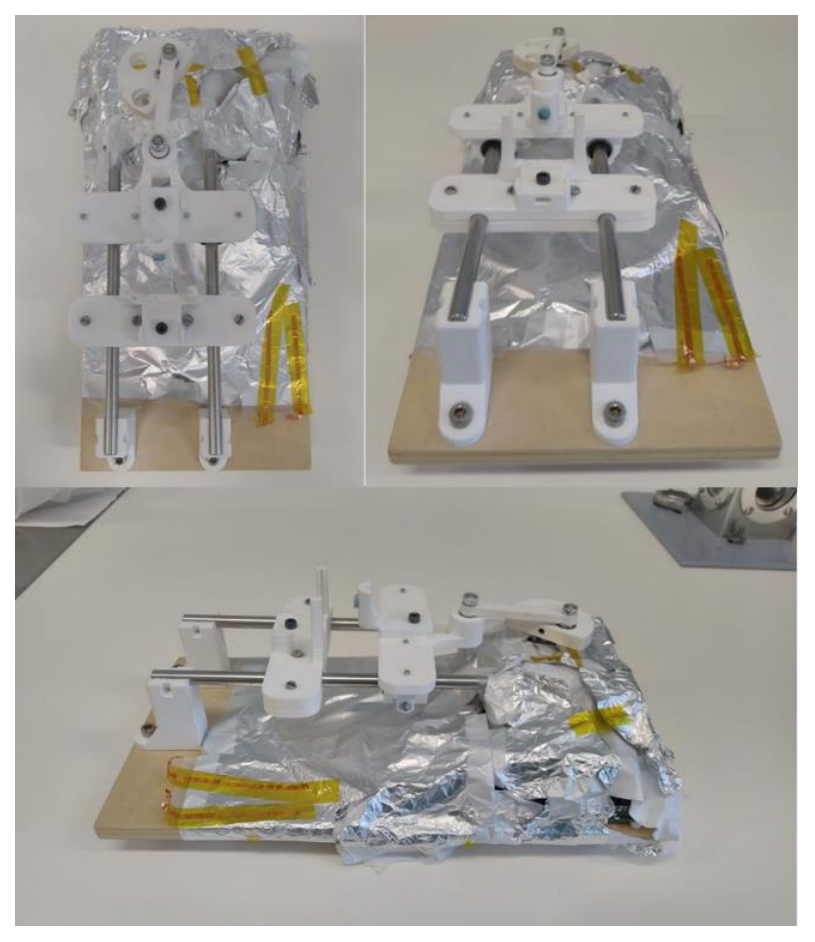


Figure A.2 - Three photographs of the home-made bending machine.

The aluminium foil around the home-made bending machine was used to reduce the electrical noise. The two copper strips were used as the ground in the electrical circuit.

The support on which the EHDs were placed to be tested, Figure A.3, is a glass piece with the force sensor attached. The glass is then inserted in a specific slot in the home-made bending machine, in order to be ready to receive impacts.

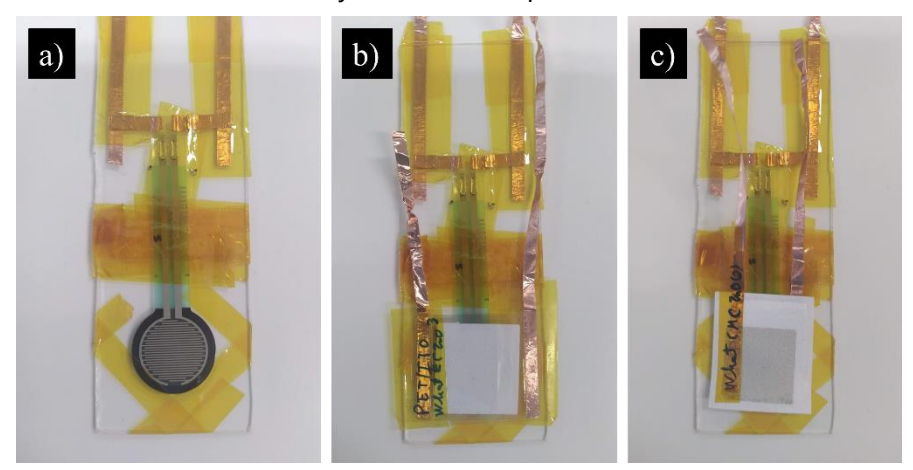


Figure A.3 - Three photographs of the support for the EHD to be place. In **a)** without an EHD, with the force sensor in sight, in **b)** with an EHD with PET/ITO electrodes, and in **c)** with an EHD with Ag electrodes, both structures made in this dissertation.

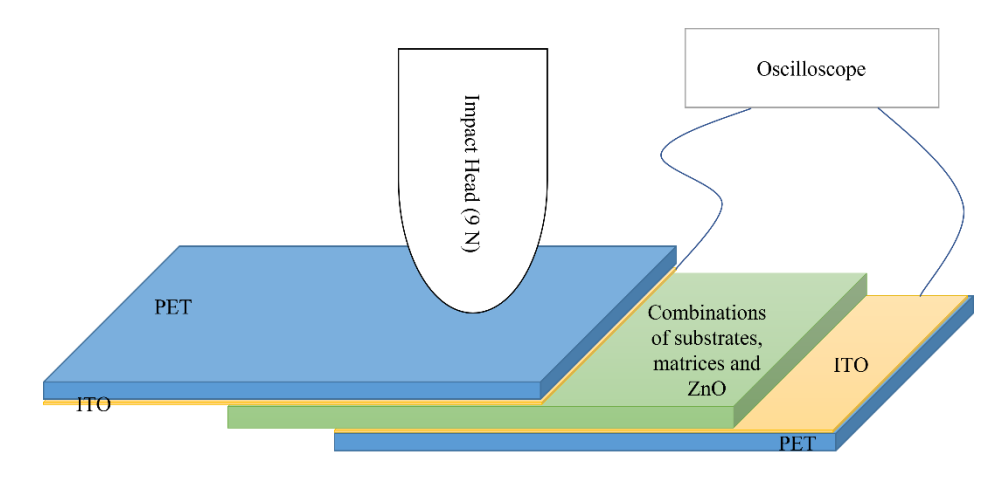


Figure A.4 - Schematic representation of the impact head hitting the EHD. Image not to scale.

### A.3 SEM

The ZnO rods here produced were observed with the help from the equipment, SEM Hitachi TM3030Plus. The images were obtained on the mix mode with an acceleration electron tension of 15 kV, with different magnifications.

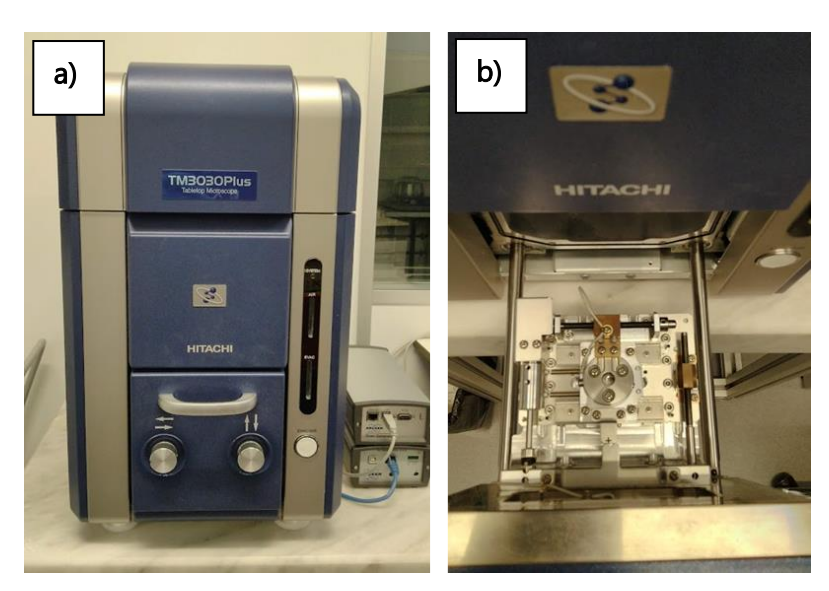


Figure A.5 - SEM equipment used for morphological and structural analysis of the EHDs and ZnO rods. In **a)** the outside of the equipment and in **b)** the inner drawer to insert the samples to be analysed.

#### Software for measurements:

Using the software ImageJ (version: 1.53k, available in https://imagej.nih.gov/ij/), the measurements for the ZnO rods length and width, and the thickness of all substrates produced, were made.

# A.4 Characterization Techniques Specifications: XRD

The structural characterization of the ZnO rods produced here was done using a PANalytical X'Pert PRO MRD diffractometer with Cu K $\alpha$  radiation. The XRD data was acquired between the angles of diffraction of 20° to 80° 20 with a step size of 0.0334°.

# A.5 Table with all data from all EHDs

In Table A.1, the global data is reunited to facilitate the comparison between certain type of EHDs produced. Showing the EHD type, and respective quantity, average peak-to-peak voltage in V and the average error in percentage associated. In total, 116 EHDs were created, comprising 32 different types of EHDs with various structures and/or compositions.

Table A.1 - Global list of the EHD produced over the course of this thesis.

FIID to ma	0 111	Average Peak-to-Peak	Average
EHD type	Quantity	Voltage (V)	Error
Control			
Ag Navigator	2	0.072	13 %
Ag Whatman	2	0.160	14 %
PET/ITO Navigator	2	1.882	3 %
PET/ITO Whatman	2	1.592	4 %
PET/ITO PDMS	5	0.486	12 %
PET/ITO CMC	3	-	-
PET/ITO EC	3	-	-
PET/ITO without ZnO	1		
PET/ITO Navigator PDMS	4	0.715	23 %
PET/ITO Whatman PDMS	4	0.975	9 %
PET/ITO Navigator CMC	4	0.623	16 %
PET/ITO Whatman CMC	4	1.713	53 %
PET/ITO Navigator EC	4	0.643	4 %
PET/ITO Whatman EC	4	0.626	15 %
PET/ITO with ZnO		'	1
PET/ITO PDMS ZnO	3	0.846	2 %
PET/ITO CMC ZnO	3	0.247	9 %
PET/ITO EC ZnO	3	2.001	46 %
PET/ITO Navigator CMC ZnO	3	0.571	20 %
PET/ITO Whatman CMC ZnO	3	1.419	43 %
PET/ITO Navigator EC ZnO	3	3.073	38 %
PET/ITO Whatman EC ZnO	3	3.493	19 %

EHD type	Quantity	Average Peak-to-Peak Voltage (V)	Average Error
Ag without ZnO			
Ag Navigator PDMS	5	0.824	3 %
Ag Whatman PDMS	5	0.756	10 %
Ag Navigator CMC	4	-	-
Ag Whatman CMC	4	-	-
Ag Navigator EC	4	0.161	11 %
Ag Whatman EC	4	0.162	10 %
Ag with ZnO			
Ag Navigator PDMS ZnO	7	0.576	4 %
Ag Whatman PDMS ZnO	6	0.555	11 %
Ag Navigator CMC ZnO	3	0.173	23 %
Ag Whatman CMC ZnO	3	0.090	8 %
Ag Navigator EC ZnO	3	0.188	5 %
Ag Whatman EC ZnO	3	0.290	5 %

### A.6 EHDs

In Figure A.6, cross section SEM images from the EHDs built with all combinations between the three matrices with ZnO rods and the two substrates are presented, all produced with Ag electrodes.

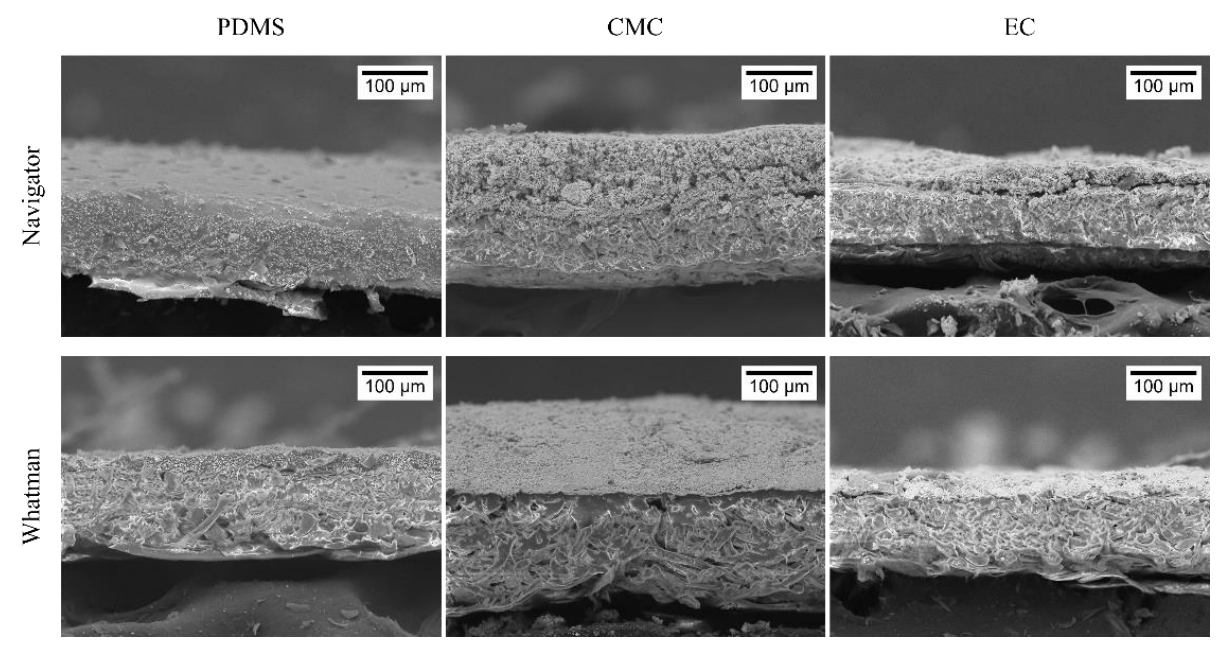


Figure A.6 - Six cross section SEM images from the devices with ZnO rods embedded in the matrices. Horizontally the two substrates, Navigator and Whatman, and vertically the three matrices, PDMS, CMC and EC.

In Figure A.7, four photographs of the EHDs produced with PDMS mixed with the ZnO rods are shown. In **a**) and **c**) on the substrate Navigator and in **b**) and **d**) the substrate Whatman. Two photographs from each EHD, one from the side where the mixture was applied and from the opposite side. The EHD build with the substrate Navigator received a UV treatment to enhance the adhesion of the Ag electrode. The photographs in **a**) and **b**) were from the side of application of the mixture by the automatic film applicator, and it is visible in **b**) that the surface is rugous, unlike the EHD with Navigator where the rugous side was the side opposite from deposition.

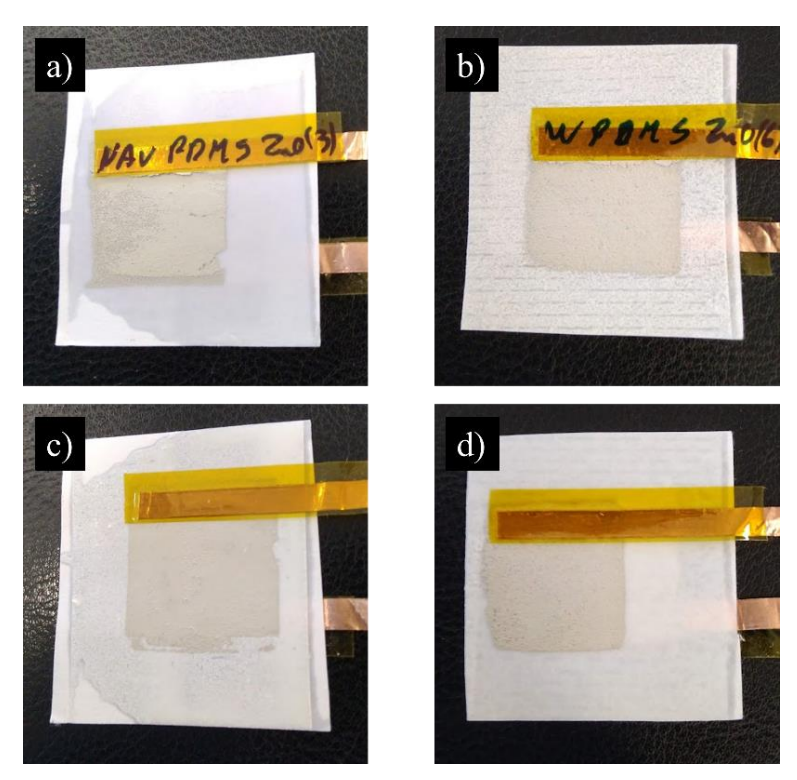


Figure A.7 - Four photographs of the EHDs build with PDMS mixed with ZnO rods, from the side where the mixture was applied and from the opposite side.

In Figure A.8, four photographs from the EHD with only PDMS deposited on the substrates, Navigator in **a**) and **c**), and Whatman in **b**) and **d**), it is observed that the surface on the substrate Navigator looks shiny, due to the lor porosity of the paper itself, against the substrate Whatman where this aspect is less noticeable.

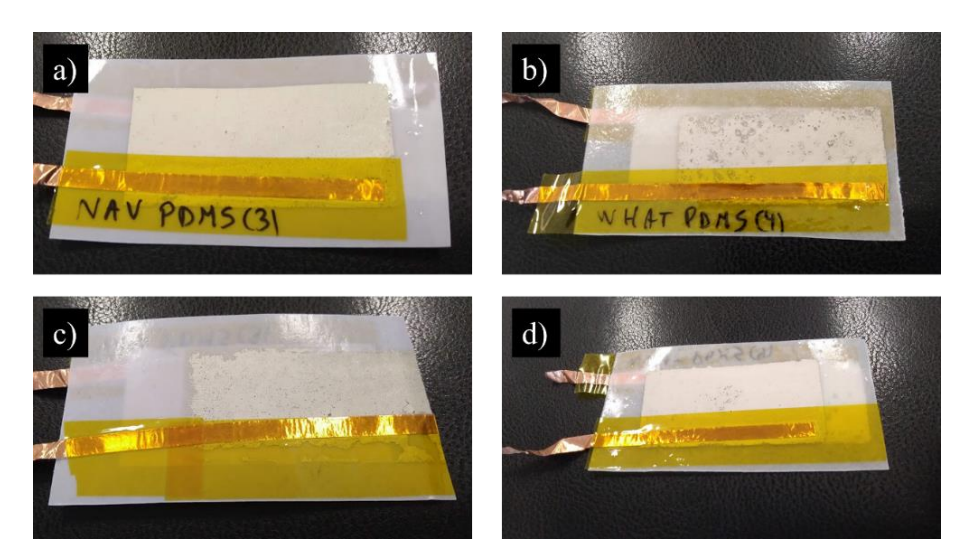


Figure A.8 - Four photographs of the EHDs build with PDMS deposited on the substrates, in **a**) and **c**) the substrate Navigator and in **b**) and **d**) the substrates Whatman.

# A.7 Future Perspectives

As seen in the literature, there are several cases of structured devices for energy harvesting, therefore, a similar approach can be taken here with the celluloses embedded in the substrates. After the deposition of the celluloses onto the substrates, they need to dry. If the embedded substrate dries within a close wavy surface, maybe made with 3D printing, and then sandwiched between the electrodes.

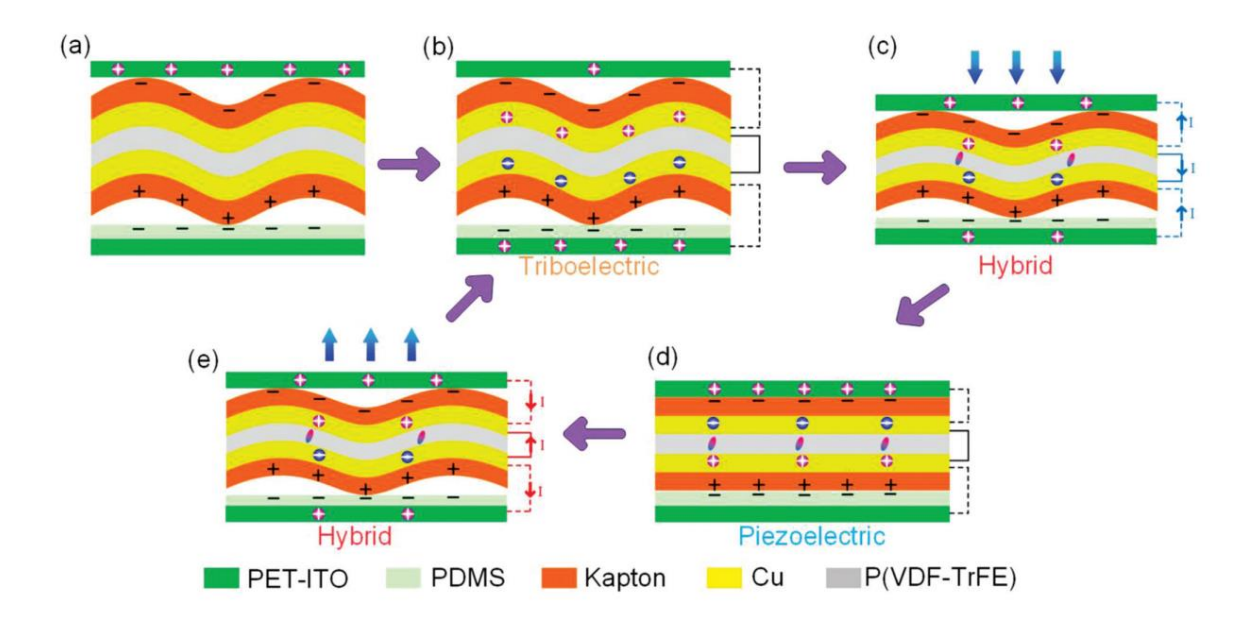


Figure A.9 - Working principle of the hybrid NG, with the wavy substrates, being an example of how a EHDs can be built in future works. Image from [32].



**TIAGO SILVA**